Cell Reports

Article

Spinal Inhibitory Ptf1a-Derived Neurons Prevent Self-Generated Itch

Graphical Abstract

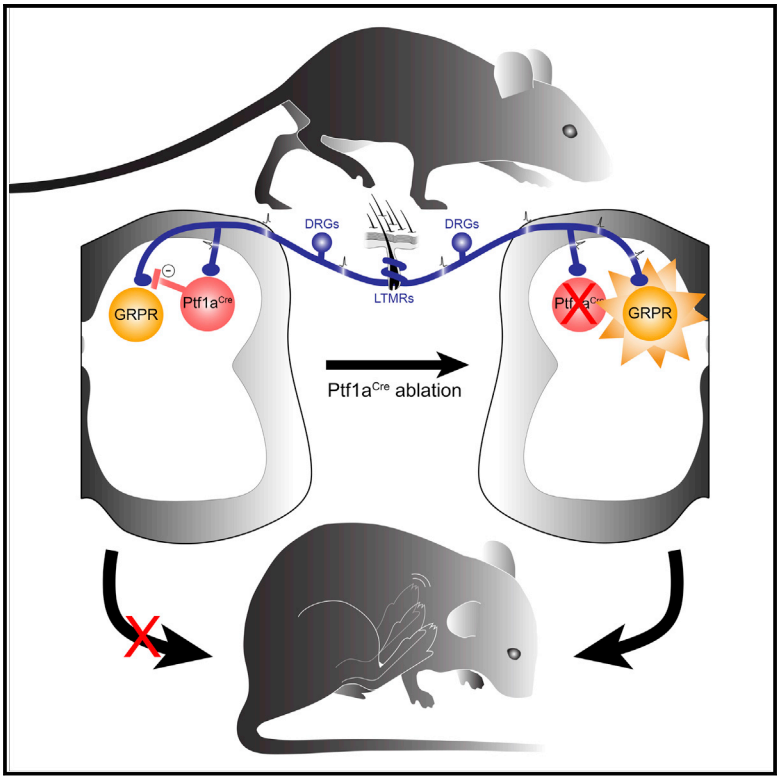

Authors

Augusto Escalante, Rüdiger Klein

Correspondence

aescalante@neuro.mpg.de (A.E.),
rklein@neuro.mpg.de (R.K.)

In Brief

To detect external stimuli, sensory systems must be able to ignore self-generated stimuli. Here, Escalante and Klein define a key role of spinal, inhibitory Ptf1a-Cre neurons as gatekeepers of self-generated mechanosensory information: absence of these neurons opens the gate for mechanical stimuli generated during movement to activate GRPR itch neurons, triggering a chronic itch state.

Highlights

- Ablation of spinal inhibitory Ptf1a-Cre neurons leads to spontaneous scratching
- Scratching is a response to self-stimulation during the animals' movements
- Ptf1a-Cre neurons receive mechanosensory and motor inputs
- Ptf1a-Cre neurons inhibit the GRPR neuron itch circuit

Escalante & Klein, 2020, Cell Reports *33*, 108422
November 24, 2020
https://doi.org/10.1016/j.celrep.2020.108422

CellPress

Cell Reports

CellPress
OPEN ACCESS

Article

Spinal Inhibitory Ptf1a-Derived Neurons Prevent Self-Generated Itch

Augusto Escalante[1,2,*] and Rüdiger Klein[1,3,*]
[1]Department Molecules-Signaling-Development, Max Planck Institute of Neurobiology, Am Klopferspitz 18, 82152 Martinsried, Germany
[2]Present address: Instituto de Neurociencias (CSIC-UMH), Developmental Neurobiology Unit, Campus de San Juan, 03550 San Juan de Alicante, Spain
[3]Lead Contact
*Correspondence: aescalante@neuro.mpg.de (A.E.), rklein@neuro.mpg.de (R.K.)
https://doi.org/10.1016/j.celrep.2020.108422

SUMMARY

Chronic itch represents an incapacitating burden on patients suffering from a spectrum of diseases. Despite recent advances in our understanding of the cells and circuits implicated in the processing of itch information, chronic itch often presents itself without an apparent cause. Here, we identify a spinal subpopulation of inhibitory neurons defined by the expression of Ptf1a, involved in gating mechanosensory information self-generated during movement. These neurons receive tactile and motor input and establish presynaptic inhibitory contacts on mechanosensory afferents. Loss of Ptf1a neurons leads to increased hairy skin sensitivity and chronic itch, partially mediated by the classic itch pathway involving gastrin-releasing peptide receptor (GRPR) spinal neurons. Conversely, chemogenetic activation of GRPR neurons elicits itch, which is suppressed by concomitant activation of Ptf1a neurons. These findings shed light on the circuit mechanisms implicated in chronic itch and open novel targets for therapy developments.

INTRODUCTION

Itch is defined as an unpleasant sensation that elicits the need to scratch (Hafenreffer, 1660). Despite its high prevalence and its health and economic burden (Kini et al., 2011; Schut et al., 2019; Tripathi et al., 2019; Weisshaar et al., 2019), itch remains a disease without a cure and with only ineffective treatments to date (Oetjen et al., 2017). Under physiological conditions, chemical itch is initiated by receptors located in the skin, which react to a plethora of chemical substances (Dong and Dong, 2018; Jakobsson et al., 2019). Conversely, mechanical itch is triggered by light tactile stimuli, such as the sensation of an insect crawling across the skin. Mechanical itch is also a widespread phenomenon associated with many skin, systemic, neurological, and psychiatric diseases (Misery et al., 2018; Mollanazar et al., 2016; Wahlgren et al., 1991; Yosipovitch and Bernhard, 2013). However, in healthy humans, it has only been unequivocally induced under laboratory experimental conditions (Fukuoka et al., 2013; Ikoma et al., 2005) or under high-intensity vibration (Mueller et al., 2019). Thus, identifying and understanding the neural circuits mediating itch responses to mechanical stimuli remain challenges.

Excitatory spinal neurons expressing the gastrin-releasing peptide receptor (GRPR) are required for itch sensation (Sun and Chen, 2007; Sun et al., 2009). GRPR neuron activity is controlled by dorsal inhibitory neurons lost in bHLH5b knockout mice (Kardon et al., 2014; Ross et al., 2010). Recent evidence indicates that only chemical, not mechanical, itch signals are conveyed through the GRPR pathway. Excitatory spinal neurons expressing the neuropeptide Y (NPY) 1 receptor specifically drive mechanical itch and are inhibited by NPY-expressing interneurons (Acton et al., 2019; Bourane et al., 2015a). NPY neurons gate yet another population of excitatory spinal neurons expressing Urocortin-3 (Ucn3). Reduced inhibition and increased excitation of Ucn3 neurons lead to chronic itch (Pan et al., 2019). However, the role of NPY in pain sensation, the co-expression of somatostatin in Ucn3-positive neurons, and the distribution of NPY receptors in both sensory fibers and spinal neurons (Jakobsson et al., 2019; Nelson et al., 2019) point to more complex functions of the NPY system in somatosensation. Whether NPY neurons are the only inhibitory neurons that gate mechanical itch remains unclear. Moreover, the nature of the stimulus triggering spontaneous mechanical itch, and resulting in self-inflicted skin wounds, has remained elusive.

Among inhibitory systems, presynaptic inhibition plays a fundamental role in modulating various types of sensory afferents (Azim et al., 2014; Fink et al., 2014; Rudomin, 2009; Rudomin and Schmidt, 1999; Zimmerman et al., 2019). Presynaptic inhibition is thought to reduce gain at sensory synapses and filter out irrelevant and self-generated sensory cues to preserve the ability to generate adequate responses to environmental stimuli in many animal species (Frost et al., 2003; Poulet and Hedwig, 2006; Seki et al., 2003; Watson, 1992). In the spinal dorsal horn, inhibitory interneurons named GABApre neurons, characterized by expression of pancreas transcription factor 1a (Ptf1a), are the source of presynaptic inhibitory synapses onto ventral proprioceptive and dorsal cutaneous afferents (Betley et al., 2009). A subset of GABApre neurons control proprioceptive sensory gain to regulate fine motor tasks (Fink et al., 2014).

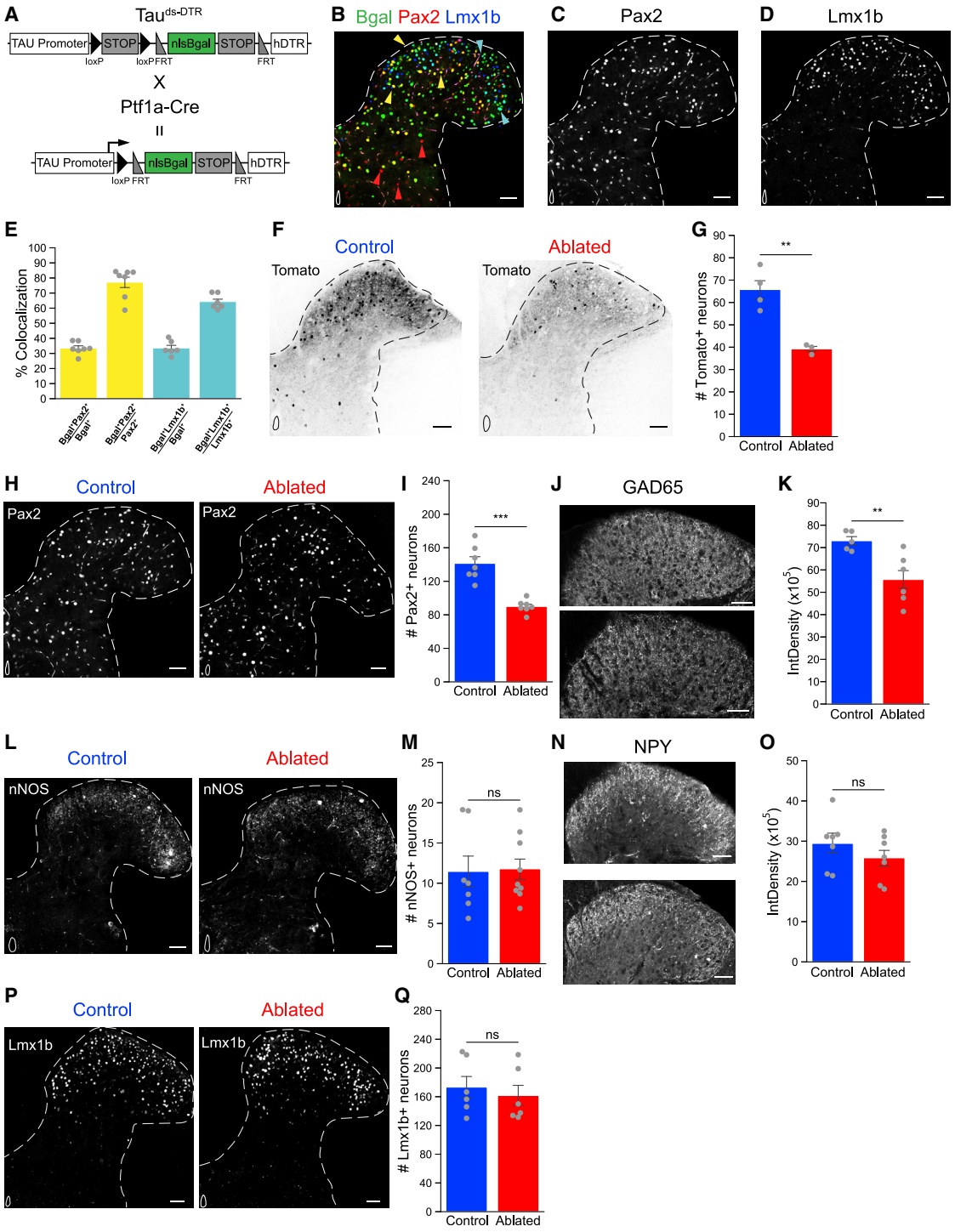

Figure 1. Targeting of a Subset of Dorsal Horn Inhibitory Neurons in Ptf1a-Cre DT-Mediated Ablation

(A) Scheme representing the Cre/Flp intersectional Tau$^{ds\text{-}DTR}$ mouse line used for DT-mediated ablation. Nuclear β-galactosidase (β-gal) expression tracks Cre^{+}/Flp^{-} neurons.

(B) Representative image of Ptf1a-Cre^{EX1};Tau$^{ds\text{-}DTR}$ adult thoracic dorsal horn section immunostained for β-gal (green), Pax2 (red), and Lmx1b (blue). Yellow arrowheads, Pax2^{+}β-gal^{+} neurons; red arrowheads, Pax2^{+}β-gal^{-} neurons ; blue arrowheads, Lmx1b^{+}β-gal^{+} neurons.

(C and D) Single channels of Pax2 (C) and Lmx1b (D) immunofluorescence from (B).

(E) Quantification of Pax2 (yellow bars), Lmx1b (blue bars), and β-gal co-localization in adult animals (n = 6–7 mice).

(legend continued on next page)

Ptf1a is transiently expressed in neural progenitors and acts as the main selector gene in establishing the dorsal interneuron 4/dorsal interneuron late A (dI4/dILA) class of spinal interneurons (Cheng et al., 2004, 2005; Glasgow et al., 2005; Gross et al., 2002; Helms and Johnson, 2003; Mizuguchi et al., 2006; Müller et al., 2002; Wildner et al., 2006). Ptf1a is required for the specification of subpopulations of inhibitory neurons implicated in itch processing: dynorphin, glycinergic transporter 2, and NPY-expressing neurons (Borromeo et al., 2014; Bröhl et al., 2008; Huang et al., 2008; Wildner et al., 2013). According to these studies, there seems to be a common link between the spinal inhibitory neurons responsible for presynaptic inhibition in the dorsal horn and the subpopulations of inhibitory neurons shown to play a role in the gating of somatosensory information. However, perinatal death of Ptf1a knockout animals has precluded further analysis into adulthood.

Here, we have used Ptf1a as a genetic entry point for manipulating these subpopulations and assessing their role in itch behavior. Our findings indicate that Ptf1a-derived inhibitory interneurons are essential components of a gating mechanism designed to block self-generated mechanosensory information. Selective, partial elimination of these neurons leads to development of the highest frequency of spontaneous-scratching behaviors described to date. We show that the scratching phenotype depends on the level of activity of the animals. Mechanistically, Ptf1a-derived interneurons control GRPR neuron-mediated itch. These results argue for Ptf1a as a common determinant of inhibitory neuron populations blocking innocuous mechanosensory input into the spinal dorsal horn. Moreover, they show that chronic itch can be a consequence of redundant innocuous tactile information.

RESULTS

Ptf1a-Cre Targets a Subset of the Inhibitory Neurons in the Spinal Dorsal Horn

To begin testing the hypothesis that Ptf1a-derived neurons constitute a subpopulation of spinal inhibitory neurons gating mechanosensory information, we first analyzed the two existing Cre recombinase knockin mouse lines: Ptf1a-Cre^{CVW} (Kawaguchi et al., 2002) and Ptf1a-Cre^{EX1} (Nakhai et al., 2007). We found that Ptf1a-derived cells were 2-fold more abundant in the Ptf1a-Cre^{EX1} than in the Ptf1a-Cre^{CVW} mouse line (Figures S1A–S1E), possibly because of better recombination efficiency (Glasgow et al., 2005). Because Ptf1a-Cre^{EX1}-derived cells recapitulated the same migration patterns previously described for Ptf1a-derived neurons in the Ptf1a-Cre^{CVW} mouse line (Glasgow et al., 2005; Meredith et al., 2009) (Figures S1F–S1J), we focused our research on the Ptf1a-Cre^{EX1} mouse line (hereafter called Ptf1a-Cre). To characterize Ptf1a-derived neurons, we used Cre-dependent nuclear expression of β-galactosidase (β-gal) present in Tau$^{ds\text{-}DTR}$ mice (Duan et al., 2014) (Figure 1A). β-gal$^+$ neurons were found in the dorsal horn (Figure 1B) overlapping with Pax2$^+$ cells, a marker of inhibitory neurons in the spinal cord (Punnakkal et al., 2014) (Figures 1C and 1E). Most Pax2$^+$ neurons expressed β-gal, but many β-gal$^+$ neurons were Pax2 negative. Co-localization with Lmx1b, a marker of excitatory neurons in the dorsal horn (Alaynick et al., 2011; Cheng et al., 2004, 2005; Dai et al., 2008; Szabo et al., 2015), indicated a similar ratio of co-expression (Figures 1D and 1E). The same percentages were observed for the Ptf1a-Cre^{CVW} mouse line (data not shown). These results suggested that Ptf1a-Cre knockin lines lack some regulatory elements to precisely recapitulate Ptf1a endogenous expression, as reported for other Cre and GFP mouse lines (Chen et al., 2011; de Chevigny et al., 2012; Dessaud et al., 2007). This scenario points to Ptf1a being transiently expressed more broadly than initially thought during development, similar to NPY reports (Bourane et al., 2015a).

To characterize the neurons targeted in Ptf1a-Cre mice, we selectively ablated them in the adult spinal cord using intersectional genetics. Combination of Ptf1a-Cre with a mouse line expressing Flp recombinase caudal to cervical segment 3 (C3) during embryogenesis, Cdx2^{FlpO} (Britz et al., 2015), and the Tau$^{ds\text{-}DTR}$ line allowed restricted expression of the human diphtheria toxin receptor (DTR) in Ptf1a-Cre spinal neurons (Figures S1K–S1O). Based on co-expression of an intersectional reporter (Madisen et al., 2015), 40% of Ptf1a-Cre neurons were ablated in the thoracic spinal cord after administration of DT compared with controls (Figures 1F and 1G). Similarly, numbers of Pax2$^+$ dorsal spinal neurons were reduced by 36% (Figures 1H and 1I), suggesting that approximately half of the 77% of Pax2 neurons derived from the Ptf1a-Cre lineage (Figure 1E) were ablated. Consistently, GAD65, the marker of GABApre presynaptic terminals in the spinal dorsal horn (Betley et al., 2009; Hughes et al., 2005; Mende et al., 2016) was decreased by 24% (Figures 1J and 1K). Markers of inhibitory neuron populations, including nNOS, NPY, galanin, and enkephalin, were unaffected (Figures 1L–1O; Figures S1P–S1R). Unexpectedly, we found an increased number of NPY- and galanin-filled somas in Ptf1a-Cre neuron-ablated animals (Figures S1S and S1T). The numbers of Lmx1b$^+$ excitatory dorsal horn neurons

(F) Representative images of adult thoracic spinal cord hemisections of control (left) and Ptf1a-Cre neuron-ablated (right) animals expressing Tomato one week after DT administration.
(G) Quantification of the number of Tomato$^+$ neurons in dorsal hemisections of control and Ptf1a-Cre neuron-ablated animals (n = 3–4 mice).
(H) Representative images of Pax2 immunofluorescence in control (left, same image as in C) and Ptf1a-Cre neuron-ablated (right) dorsal hemisections.
(I) Quantification of the number of Pax2$^+$ neurons in dorsal hemisections of control and Ptf1a-Cre neuron-ablated animals (n = 7 mice).
(J) Representative images of GAD65 immunofluorescence in control (top) and Ptf1a-Cre neuron-ablated (bottom) spinal cord dorsal horns.
(K) Quantification of GAD65 immunofluorescence in the dorsal horns of control and Ptf1a-Cre neuron-ablated animals (n = 5–6 mice).
(L) Representative images of nNOS immunofluorescence in control (left) and Ptf1a-Cre neuron-ablated (right) dorsal hemisections.
(M) Quantification of the number of nNOS$^+$ neurons in dorsal hemisections of the spinal cord in control and Ptf1a-Cre neuron-ablated animals (n = 7–9 mice).
(N) Representative images of NPY immunofluorescence in control (top) and Ptf1a-Cre neuron-ablated (bottom) spinal dorsal horns.
(O) Quantification of NPY immunofluorescence in the dorsal horns of control and Ptf1a-Cre neuron-ablated animals (n = 7 mice).
(P) Representative images of Lmx1b immunofluorescence in control (left) and Ptf1a-Cre neuron-ablated (right) dorsal hemisections.
(Q) Quantification of the number of Lmx1b$^+$ neurons in dorsal hemisections of the spinal cord in control and Ptf1a-Cre neuron-ablated animals (n = 6 mice).
Scale bars: 50 μm. Data: mean ± SEM. See also Figure S1.

were unchanged (Figures 1P and 1Q). Sensory terminals of non-peptidergic IB4$^+$ nociceptors, VGlut1$^+$ Aβ and Aδ fibers, and VGlut2$^+$ excitatory terminals were also unaltered (Figures S1S–S1U). These results indicate that Ptf1a-Cre mice selectively ablate a subpopulation of spinal inhibitory neurons with little or no overlap with previously described subtypes.

Ptf1a-Cre Neurons Receive Mechanosensory and Motor Input

The Ptf1a lineage gives rise to presynaptic inhibitory neurons, so-called GABApre neurons (Betley et al., 2009; Fink et al., 2014; Mende et al., 2016). Expression of the synaptophysin-GFP (SynGFP) fluorescent presynaptic marker in Ptf1a-Cre$^+$ neurons (Tripodi et al., 2011) (Figure 2A), showed that 84% of presynaptic inhibitory contacts on adult VGlut1$^+$ sensory terminals derive from Ptf1a neurons (Figures 2B–2D), similar to previous reports (Betley et al., 2009). After DT-mediated ablation of Ptf1a-Cre neurons, we measured an 18% decrease in the number of presynaptic inhibitory VGAT$^+$ contacts over VGlut1$^+$ terminals compared with controls in the dorsal horns (Figure 2F). These results confirm that most Ptf1a-derived adult inhibitory neurons establish presynaptic inhibitory synapses and that our ablation strategy targets a subset of them.

To gain insight into the monosynaptic inputs received by Ptf1a neurons, we performed retrograde rabies virus tracing (Wickersham et al., 2007). Ptf1a-Cre mice were crossed with RΦGT (Takatoh et al., 2013) mice, thereby expressing the auxiliary TVA and G proteins (Figures 2G and 2H) specifically in Ptf1a neurons. Immunohistochemical characterization of GFP$^+$ dorsal root ganglion (DRG) neurons (Figures 2I and 2J) revealed low-threshold mechanoreceptors (LTMRs) involved in transmission of touch information and marked by NF200$^+$ (32.04% ± 4.26%), NF200$^+$CGRP$^+$ (43.73% ± 6.85%), TrkC$^+$ (12.76% ± 0.81%), and TH$^+$ (8.86% ± 8.04%). A small percentage of them were associated with the unmyelinated peptidergic nociceptive neurons CGRP$^+$NF200$^-$ (12.6% ± 7.07%), a few were associated with the proprioceptive inputs PV$^+$ (2.12% ± 0.5%) and PV$^+$TrkC$^+$ (1.06% ± 0.63%), and none were associated with non-peptidergic nociceptors (IB4$^+$) (Bourane et al., 2015b; Lallemend and Ernfors, 2012; Usoskin et al., 2015). Ptf1a neurons also received monosynaptic inputs from supraspinal regions generally associated with descending motor pathways (Figures 2K–2M). Major contributing regions were layer V motor cortex (32.95% ± 12%), corresponding to corticospinal projection neurons involved in skilled movements (Moreno-López et al., 2016; Ueno et al., 2018), and the gigantocellular (Gi) nucleus (30.1% ± 12.33%) of the reticulospinal tract, important for motor control (Bouvier et al., 2015; Brownstone and Chopek, 2018; Capelli et al., 2017; Liang et al., 2016). Minor contributions came from the red nucleus, the medullary reticular nucleus, and the raphe nucleus (Figure 2N). In summary, these results revealed that Ptf1a-Cre neurons established presynaptic inhibitory contacts with myelinated cutaneous afferents and received direct mechanosensory and higher-order motor information.

Ablation of Ptf1a-Cre Spinal Neurons Leads to Spontaneous Scratching

To detect early behavioral alterations in Ptf1a-Cre neuron-ablated mice, we video recorded mice daily in their home cages before and after ablation. Ptf1a-Cre neuron-ablated animals developed an intense itch sensation and started to scratch only two days after DT administration, reaching peak scratching frequency one day later (Figure 3A). At day seven, animals started to develop fur loss and skin injuries, so the experiment was terminated. Scratching was mostly directed to the nape of the neck, forearm, and flanks. Rarely, we observed scratching toward the cheeks, snout, or scalp, in accordance with the limited rostral ablation imposed by the use of Cdx2^{FlpO}. In summary, Ptf1a-Cre neuron-ablated animals showed a more than 60-fold increase in scratching (Figure 3B). We observed the same phenotype using the Ptf1a-Cre^{CVW} mouse line (Figure S2A), supporting the functional specificity of Ptf1a-Cre neurons.

Spontaneous-scratching behavior developed quickly, reaching peak values 6.8 days after first DT administration (Figure 3C). Grooming time of Ptf1a-Cre neuron-ablated animals was 5-fold higher compared with DT-treated control littermates (Figure 3D). Injections of chemical histaminergic and non-histaminergic pruritogens in the back region before the onset of spontaneous scratching, but after loss of Ptf1a neurons (Figure S2B), showed no differences between control and Ptf1a-Cre neuron-ablated littermates (Figures 3E and 3F), demonstrating that the spontaneous-scratching phenotype was not related to chemical itch. Additional behavioral tests revealed no changes in the processing of other somatosensory modalities (Figures S2C–S2G), acute mechanical itch (Figures S2H and S2I), locomotor coordination (Figures S2J and S2K), or anxiety (Figure S2K). Altogether, these findings suggest that the subset of Ptf1a$^+$ inhibitory neurons targeted by Ptf1a-Cre specifically mediate mechanical itch control in the spinal dorsal horn.

Ptf1a-Cre Neurons Control Hairy Skin Sensitivity

To identify the nature of the itch-inducing stimulus, we studied the scratch response before and after removal of bedding material from the home cage. Ptf1a-Cre neuron-ablated animals decreased 40% in scratching frequency (Figure 3G), suggesting a role for mechanical stimuli in the induction of itch. We reasoned that mechanosensory stimuli causing the scratch phenotype might be detected by hairs, the most common mechanoreceptor in hairy skin, and performed an experiment to test hairy skin sensitivity to air puffs of different intensities directed toward the back of the animal (Orefice et al., 2016). The response curve to air puffs of increasing intensities for control animals treated with DT (Figure S2L) showed that the minimum intensity that elicited a significant response was 0.5 psi. Ptf1a-Cre neuron-ablated animals showed a 2-fold increased response to this threshold intensity compared with controls (Figure 3H). Ablation of Ptf1a-Cre neurons did not alter startle responses or prepulse inhibition characteristics in either the acoustic or the tactile versions of the assay (Figures S2M–S2R).

Ptf1a-Cre neuron-ablated animals showed increased activity in the spinal dorsal horns as measured by the number of cFos$^+$ neurons (Figures 3I–3K). To establish a causal relationship between hairy skin sensitivity and dorsal horn neuronal activity, avoiding the potential effect of scratching in dorsal horn activity, we designed a back hair stimulation protocol under anesthesia (Figure 3L). Spinal cords of hair-stimulated Ptf1a-Cre neuron-ablated

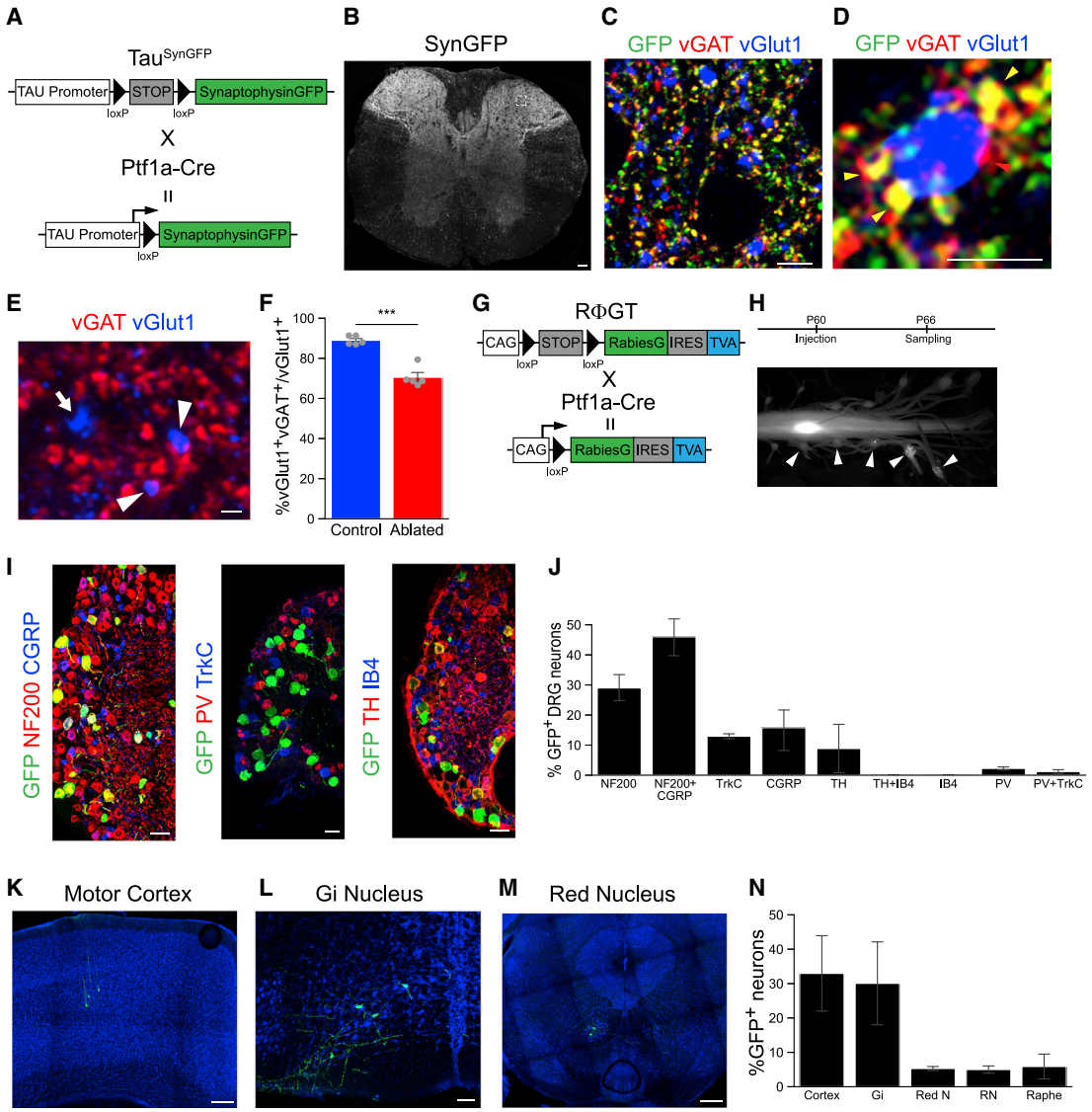

Figure 2. Mechanosensory and Motor Input to Ptf1a-Cre Presynaptic Neurons

(A) Scheme representing the genetic strategy used for the labeling of Ptf1a presynaptic terminals.

(B) Overview of GFP immunofluorescence in the thoracic spinal cord section from an adult Ptf1a-Cre;Tau$^{lsl\text{-}SynGFP}$ mouse.

(C and D) Representative image (C) of the dorsal spinal cord showing sensory terminals (VGlut1$^+$, blue) receiving presynaptic inhibitory contacts (VGAT$^+$, red). A high proportion are Ptf1a-derived GFP$^+$ (green). High-magnification image (D) showing a single sensory terminal expressing VGlut1$^+$ (blue) contacted by several presynaptic inhibitory terminals (VGAT$^+$, red). Some are derived from Ptf1a neurons (GFP$^+$, yellow arrowheads), and one comes from a non-Ptf1a-derived VGAT$^+$GFP$^-$ terminal (red arrowhead) (n = 3 mice).

(E) Representative image of the dorsal spinal cord showing sensory terminals (VGlut1$^+$, blue) receiving presynaptic inhibitory contacts (VGAT$^+$, red; arrowheads). The arrow points to a single VGlut1$^+$ sensory terminal devoid of presynaptic inhibitory contacts.

(F) Quantification of the percentage of VGlut1$^+$ sensory terminals apposed by VGAT$^+$ inhibitory synapses in the dorsal horn of control (blue) and Ptf1a-Cre neuron-ablated (red) animals (n = 5 mice).

(G) Scheme representing the RΦGT mouse line used for transsynaptic tracing with EnvA-pseudotyped rabies virus. Cre recombination leads to the expression of rabies G protein and TVA.

(H) Spinal cords, DRGs, and brains were processed for immunofluorescence 6 days after injection. Bottom panel: whole-mount image of caudal spinal cord 6 days after injection with EnvA-pseudotyped rabies virus. Arrowheads indicate DRGs with GFP$^+$ sensory neurons.

(I) Representative images of DRGs showing GFP$^+$ neurons labeled by transsynaptic tracing from Ptf1a-Cre neurons. Neurofilament (NF200), calcitonin gene-related peptide (CGRP), parvalbumin (PV), tropomyosin receptor kinase C (TrkC), tyrosine hydroxylase (TH), and isolectin GS-IB$_4$ (IB4) immunofluorescence.

(J) Quantification of GFP co-localization with sensory neuron markers expressed as a percentage of the total of GFP$^+$ neurons (n = 3 mice per marker combination).

(K–M) Representative images of GFP$^+$ cortical (K), Gi nucleus (L), and red nucleus (M) neurons labeled by transsynaptic tracing from Ptf1a spinal neurons.

(N) Quantification of supraspinal input regions to Ptf1a spinal neurons expressed as a percentage of the total of GFP$^+$ neurons found in the brain (n = 5 mice).

Scale bars: (B and I) 50 μm, (K and M) 200 μm, (L) 100 μm, (C) 5 μm, (D) 2.5 μm, (E) 1 μm. Data: mean ± SEM.

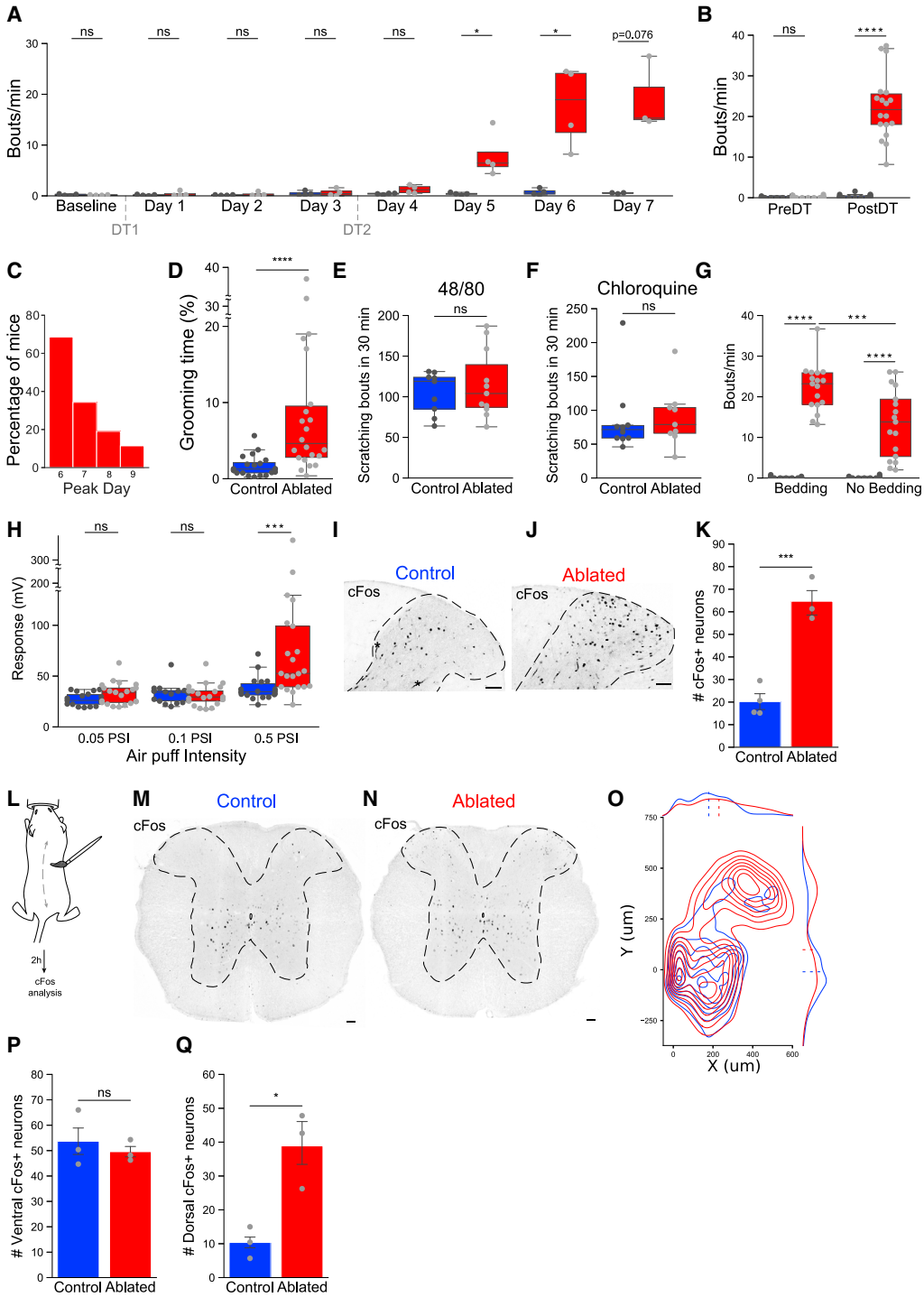

Figure 3. Spontaneous Scratching and Increased Hairy Skin Sensitivity upon Loss of Ptf1a-Cre Neurons

(A) Time course of the spontaneous-scratching phenotype in control (blue) and Ptf1a-Cre neuron-ablated (red) animals. DT1 and DT2 depict the times of DT administration. n = 4 animals per group and time point. Day 7 only includes 3 animals because of the sacrifice of one animal according to ethical considerations. Two-sided Mann-Whitney's unpaired U test.

(B) Quantification of scratching frequency in control (blue) and Ptf1a-Cre neuron-ablated (red) animals in home cages before and after DT treatment (n = 16–18 mice). Two-sided Mann-Whitney's unpaired U test.

(C) Histogram representing the percentage of Ptf1a-Cre neuron-ablated animals at maximum scratching frequency in relation to time after DT1 (n = 35 mice).

(legend continued on next page)

animals showed a localized increase of cFos$^+$ neurons in the dorsal horns that was almost 4-fold higher than in control animals (Figures 3M–3O). The number of cFos$^+$ neurons in the ventral spinal cord, a region not innervated by cutaneous afferents, did not change (Figures 3P and 3Q). These results support the idea that spontaneous scratching observed in Ptf1a-Cre neuron-ablated animals is a response to mechanical hair stimulation normally inhibited by Ptf1a-Cre neurons under physiological conditions.

Mouse Activity Correlates with Scratching in Ptf1a-Cre Neuron-Ablated Animals

In the pursuit of understanding the scratching behavior of Ptf1a-Cre neuron-ablated animals in a naturalistic environment for laboratory mice (Babayan and Konen, 2019), we designed a system to continuously video record mice in their home cages for several days without human intervention (Figure 4A). A combination of various machine-learning methods was used to extract the frames in which the animal performed scratching behavior and to analyze the resulting data (Figures S3A–S3D). Our aim was to understand whether there were differences in the intensity of the phenotype depending on the circadian phase, which correlates with animal activity, and whether we could explain the association between hairy skin and scratching.

The level of activity, measured as speed of the animals, oscillated accordingly with changes in the light cycle for both control and ablated animals (Figures 4B and 4C; Figures S3E–S3G). We found that scratching times changed in agreement with the light phases for both control and Ptf1a-Cre neuron-ablated animals (Figure 4D) except at the end of the experiment, when Ptf1a-Cre neuron-ablated animals had developed peak scratching behavior and scratching frequency remained high even during the light phase (Figure 4E; Figures S3H and S3I). Individual analysis of the scratching trajectories for each animal clearly showed increased scratching frequency during the dark phases, which corresponded to higher activity (Figures 4F and 4G). We postulated a link between the level of activity of the animal and the intensity of the scratching phenotype, because movement of the animal would inescapably lead to self-activation of its own hairs. A clear correlation between variables was observed for control animals (Figure 4H) and to a lesser extent for Ptf1a-Cre neuron-ablated animals (Figure 4I), which showed higher variability in scratching behavior. To test the idea that animal activity and scratching frequency were related, we evaluated scratching frequencies in two contexts: active and resting (see STAR Methods). Ptf1a-Cre neuron-ablated animals in the active context scratched 4 times more often than those in the resting context (Figure 4J). Control animals also reduced scratching in the resting context, but at a reduced level (Figure 4J). Each animal tested showed decreased scratching frequency in the resting context (Figure 4K). These results are in agreement with the behavior in the long-term analysis presented earlier. However, it is possible that higher scratching in the first (active) context resulted from increased anxiety, not general activity. To rule out this possibility, we placed mice in the same holding cylinder used for air puff delivery (as in Figure 3J), a context with higher anxiety potential than the open home cage. Ptf1a-Cre neuron-ablated animals reduced scratching behavior more than 60-fold when placed in the cylinder, a context in which they can still move and scratch but cannot walk freely (Figures 4L and 4M). Altogether, these results favor the idea that the spontaneous scratching observed after Ptf1a-Cre neuron ablation is an exacerbated response to self-stimulation of fur generated during normal activity of the animal.

GRPR$^+$ Neurons Partially Mediate Scratching after Ptf1a-Cre Neuron Ablation

To elucidate whether GRPR neurons are involved in the scratching phenotype of Ptf1a-Cre neuron-ablated animals, we used a GRPR-specific antagonist (Pereira et al., 2015; Sukhtankar and Ko, 2013). Administration of the antagonist after removal of the bedding material from the home cage further reduced the scratching frequency of Ptf1a-Cre neuron-ablated animals by 50% (Figure 5A). In agreement with a model in which GRPR neuronal activity is involved in the scratching behavior of Ptf1a-Cre neuron-ablated mice, we found that 86% of VGlut1$^+$ terminals contacting GRPR-Cre neurites received VGAT$^+$ presynaptic inhibitory contacts, most likely coming from Ptf1a neurons (Figure 5B). To obtain genetic evidence for the role of GRPR-Cre neurons, we compared the scratching phenotype of Ptf1a-Cre neuron-ablated mice with that of mice in which both

(D) Quantification of the time spent grooming by control (blue) and Ptf1a-Cre neuron-ablated (red) animals in home cages after DT treatment (n = 20–22 mice). Two-sided Mann-Whitney's unpaired U test.
(E and F) Quantification of scratching frequency in control (blue) and Ptf1a-Cre neuron-ablated (red) animals after injection of compound 48/80 (E) or chloroquine (F) in the back 5 days after DT1 (n = 9–11 mice). Two-sided Mann-Whitney's unpaired U test.
(G) Quantification of scratching frequency in control (blue) and Ptf1a-Cre neuron-ablated (red) animals in home cages 30 min after removal of bedding material (n = 14–17 mice). Two-sided Mann-Whitney's unpaired U test and two-sided Wilcoxon's signed-rank paired test.
(H) Quantification of the activity response elicited by air puffs of increasing intensity directed toward the back of control (blue) and Ptf1a-Cre neuron-ablated (red) animals 5 days after DT1 (n = 12–21 mice). Two-sided Mann-Whitney's unpaired U test.
(I and J) Representative images of cFos immunofluorescence in control (I) and Ptf1a-Cre neuron-ablated (J) spinal cord dorsal hemisections after DT. Asterisks, blood vessels.
(K) Quantification of the number of cFos$^+$ neurons in dorsal hemisections in control and Ptf1a-Cre neuron-ablated animals (n = 3–4 mice).
(L) Schematic representation of cFos induction through fur stimulation.
(M and N) Representative images of cFos immunofluorescence in control (M) and Ptf1a-Cre neuron-ablated (N) spinal cord sections after DT treatment and fur stimulation protocol.
(O) Kernel density estimate plot of the distribution of cFos$^+$ neurons in control (blue, n = 3 mice, 3,075 neurons) and Ptf1a-Cre neuron-ablated (red, n = 3 mice, 3,957 neurons) spinal cords after fur stimulation.
(P and Q) Quantification of the number of cFos$^+$ neurons in ventral (P) and dorsal (Q) spinal cord from control (blue) and Ptf1a-Cre neuron-ablated (red) animals after fur stimulation (n = 3 mice).
Scale bars: 50 μm. Data: mean ± SEM. See also Figure S2.

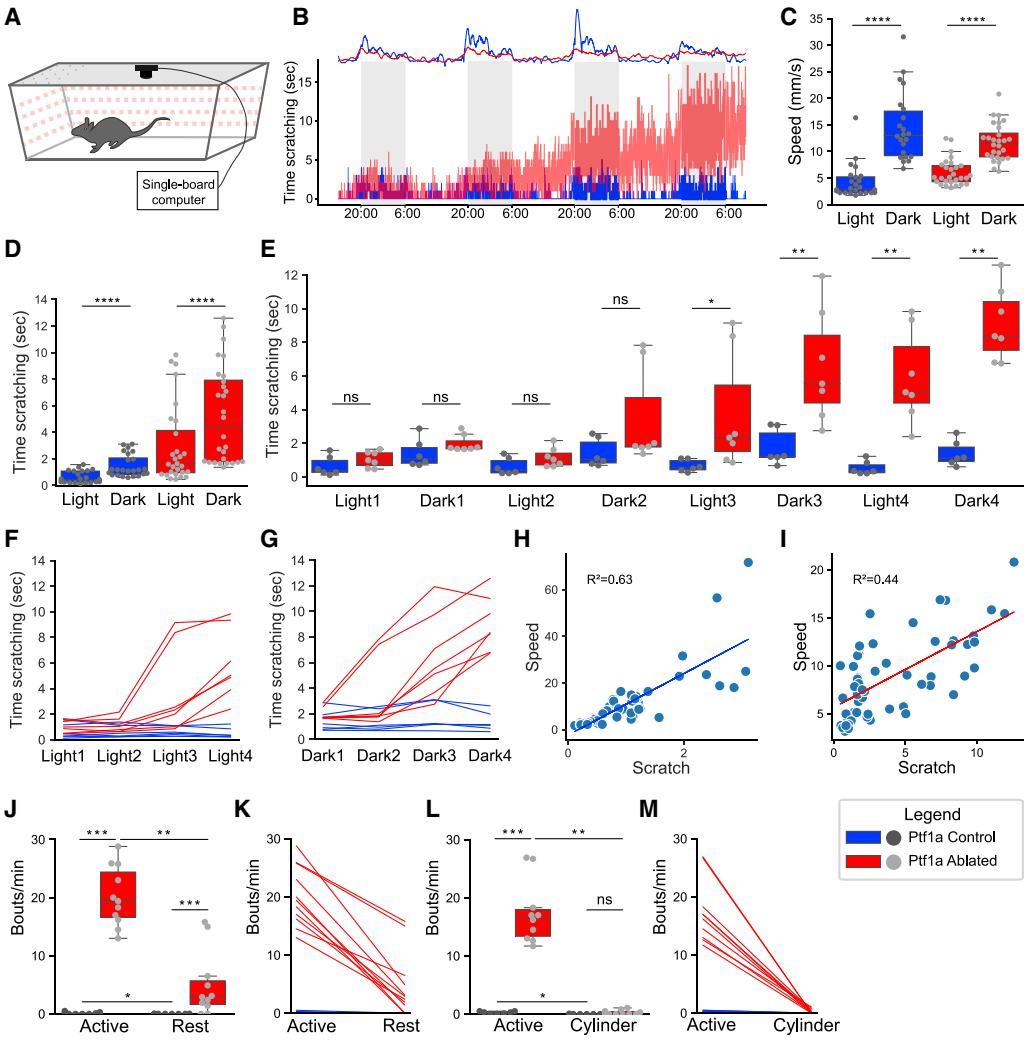

Figure 4. Scratching in Ptf1a-Cre Neuron-Ablated Animals Depends on Animal Activity

(A) Schematic representation of the setup used to record the activity of single-housed mice continuously for several days (see STAR Methods for details).

(B) Graphical representation of the time spent scratching as a function of time. Top panel: average speed for control (blue n = 6 mice) and Ptf1a-Cre neuron-ablated (red, n = 7 mice) animals. Bottom panel: average scratching time per minute for control (blue, n = 6 mice) and Ptf1a-Cre neuron-ablated (red, n = 7 mice) animals. Two-sided Mann-Whitney's unpaired U test. Gray shadows represent the dark phase of the light cycle.

(C) Mean speed in control (blue, n = 6 mice) and Ptf1a-Cre neuron-ablated (red, n = 7 mice) animals during light and dark phases. Two-sided Wilcoxon's signed-rank paired test.

(D) Mean scratching time per minute in control (blue, n = 6 mice) and Ptf1a-Cre neuron-ablated (red, n = 7 mice) animals during light and dark phases. Two-sided Wilcoxon's signed-rank paired test.

(E) Scratching time per minute in each light/dark phase for control (blue, n = 6 mice) and Ptf1a-Cre neuron-ablated (red, n = 7 mice) animals during the entire length of the video recordings. Two-sided Mann-Whitney's unpaired U test: $^{ns}p > 0.05$, $^{*}p < 0.05$, $^{**}p < 0.01$.

(F and G) Time course of mean scratching time in each light (F) and dark (G) phase for control (blue, n = 6 mice) and Ptf1a-Cre neuron-ablated (red, n = 7 mice) animals.

(H and I) Ordinary linear regression analysis model fitting for scratching and speed data of control (n = 6 mice, (H) and Ptf1a-Cre neuron-ablated (n = 7 mice, I) animals during each cycle phase for the whole study.

(J) Scratching frequency in control (blue, n = 10 mice) and Ptf1a-Cre neuron-ablated (red, n = 11 mice) animals at the peak day in home cages (active) and 30 min after returning them to their respective racks (rest). Two-sided Mann-Whitney's unpaired U test and two-sided Wilcoxon's signed-rank paired test.

(K) Individual mouse representation of data in (G) for control (blue lines) and Ptf1a-Cre neuron-ablated (red lines) animals.

(L) Scratching frequency in control (blue, n = 7 mice) and Ptf1a-Cre neuron-ablated (red, n = 10 mice) animals at the peak day in their home cages (active) and 1 h later inside the startle response cylinder (cylinder). Two-sided Mann-Whitney's unpaired U test and two-sided Wilcoxon's signed-rank paired test.

(M) Individual mouse representation of data in (I) for control (blue lines) and Ptf1a-Cre neuron-ablated (red lines) animals.

Data: mean ± SEM. See also Figure S3.

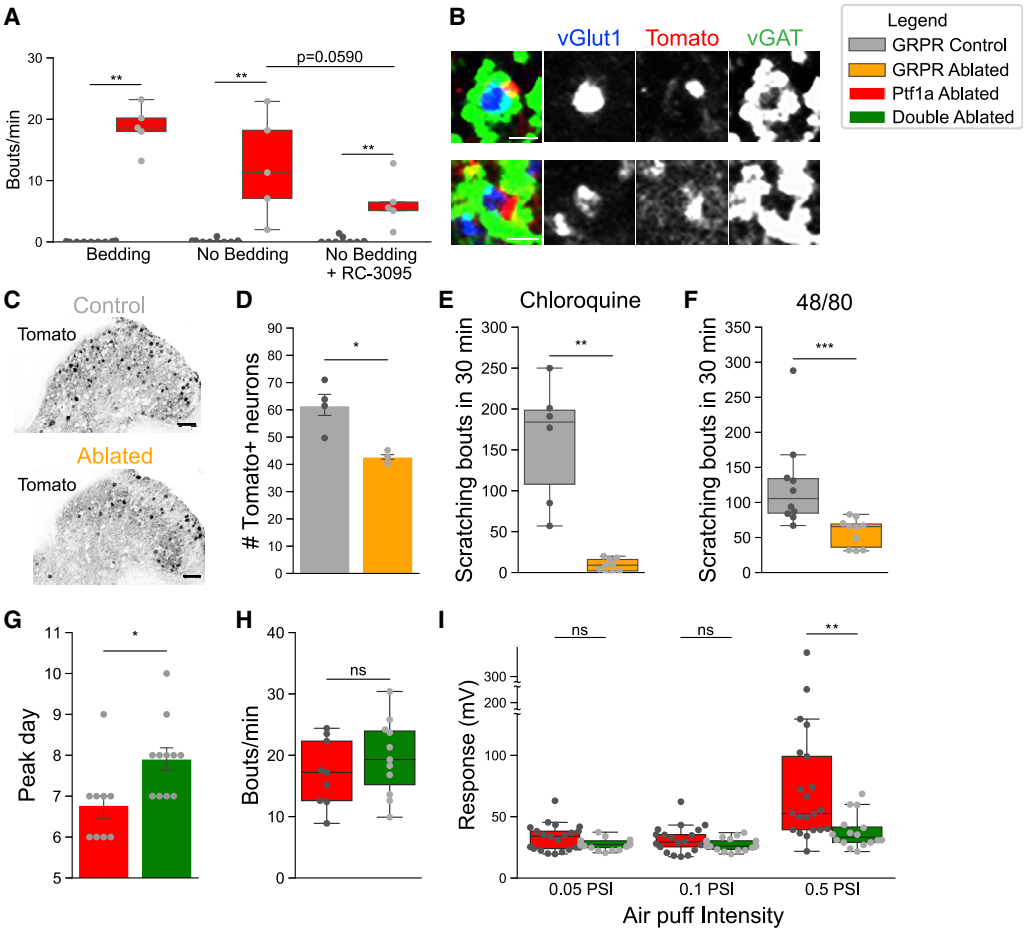

Figure 5. Spinal GRPR$^+$ Neurons' Role in Ptf1a-Cre Neuron-Ablated Scratching

(A) GRPR antagonist RC-3095 effects on scratching frequency in control (blue, n = 9 mice) and Ptf1a-Cre neuron-ablated (red, n = 5 mice) animals. Two-sided Mann-Whitney's unpaired U test and two-sided Wilcoxon's signed-rank paired test.

(B) Representative images of GRPR-Cre;Ai9$^{lsl\text{-}tdTomato}$ neurites contacting VGlut1$^+$ somatosensory terminals apposed with VGAT$^+$ inhibitory puncta (n = 3 animals).

(C) Representative images of adult thoracic spinal cord hemisections of control (top) and GRPR-Cre neuron-ablated (bottom) animals expressing Tomato one week after DT administration.

(D) Numbers of Tomato$^+$ neurons in spinal dorsal hemisections in control (gray, n = 4 mice) and GRPR neuron-ablated (orange, n = 3 mice) animals.

(E and F) Quantification of scratching bouts in control (gray, n = 6 mice) and GRPR neuron-ablated (orange, n = 10 mice) animals after injection of chloroquine (E) or compound 48/80 (F) in the back. Two-sided Mann-Whitney's unpaired U test.

(G) Quantification of time after DT1 in which Ptf1a-Cre neuron-ablated (red, n = 9 mice) and Ptf1a;GRPR neuron-ablated (green, n = 11 mice) animals reached maximum scratching frequency. Two-sided Mann-Whitney's unpaired U test.

(H) Quantification of scratching frequency in Ptf1a-Cre neuron-ablated (red, n = 9 mice) and Ptf1a;GRPR neuron-ablated (green, n = 11 mice) animals in home cages at the peak day after DT treatment. Two-sided Mann-Whitney's unpaired U test.

(I) Quantification of the activity response elicited by air puffs of increasing intensity directed toward the back of Ptf1a-Cre neuron-ablated (red, as in Figure 3D) and Ptf1a;GRPR neuron-ablated (green) animals 5 days after DT1(n = 17–21 animals per group). Two-sided Mann-Whitney's unpaired U test.

Scale bar: (B) 1 μm; rest, 50 μm. Data: mean ± SEM. See also Figure S4.

Ptf1a-Cre and GRPR-Cre neurons were ablated. Ablation efficiency of GRPR-Cre neurons was partial (Figures 5C–5E) but sufficient to markedly decrease the scratching response to chemical pruritogens (Figures 5F and 5G). In agreement with previously reported data, GRPR-Cre neuron-ablated animals did not show other sensory or motor deficiencies (Figure S4) (Sun and Chen, 2007; Sun et al., 2009). Simultaneous ablation of Ptf1a-Cre and GRPR-Cre neurons delayed the development of peak scratching activity by more than one day compared with animals with only ablated Ptf1a-Cre neurons (Figure 5G) but had no effect on peak scratching frequency (Figure 5H). Moreover, the increased sensitivity of Ptf1a-Cre neuron-ablated hairy skin toward gentle air puffs returned to a normal level in double-Ptf1a-Cre;GRPR-Cre neuron-ablated animals (Figure 5I). In summary, these results suggest that Ptf1a-Cre neurons gate mechanosensory information to the GRPR and another yet-unknown excitatory itch pathway: loss of Ptf1a-Cre neurons leads to excess mechanosensory information in the circuit

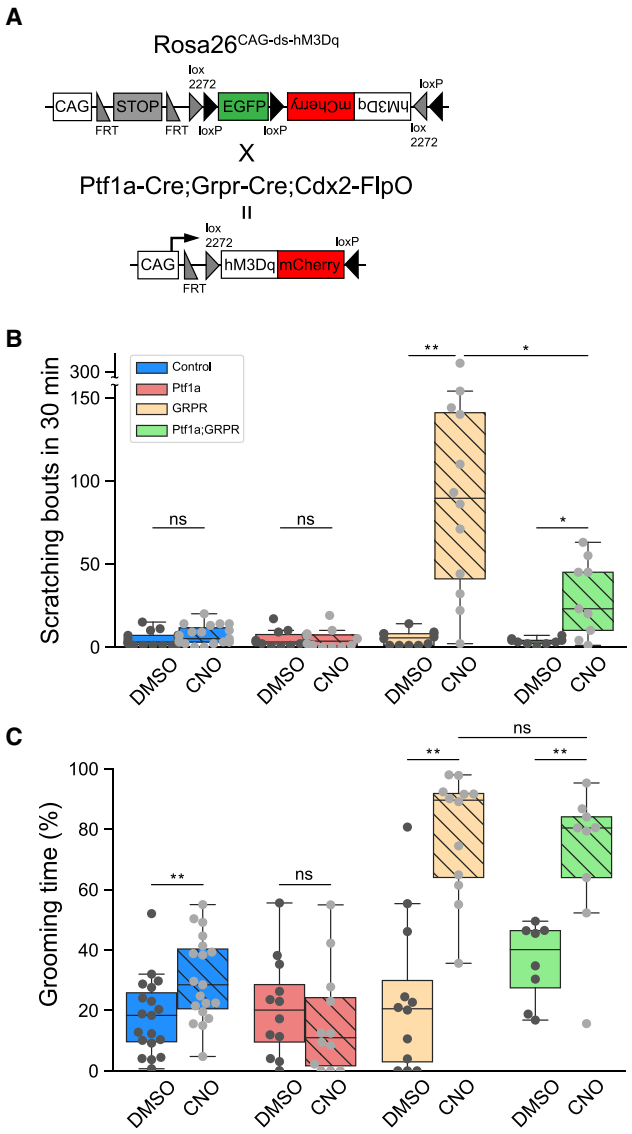

Figure 6. Ptf1a-Cre Neuron Activation Inhibits GRPR Neuron-Induced Itch

(A) Schematic representation of genetic crosses for designer receptors exclusively activated by designer drugs (DREADD)-mediated simultaneous activation of Ptf1a$^+$ and GRPR$^+$ neurons in the spinal cord.

(B) CNO-mediated activation of GRPR$^+$ neurons induces scratching (n = 12 mice), which can be reduced through simultaneous activation of GRPR$^+$ and Ptf1a$^+$ neurons (n = 9–12 mice). No differences are observed upon CNO administration to control (n = 19 mice) or Ptf1a neuron-activated (n = 12 mice) animals compared with the same animals treated with vehicle DMSO.

(C) Intense grooming induced by CNO-mediated activation of GRPR$^+$ neurons (n = 12 mice) is not compensated for by the concomitant activation of Ptf1a$^+$ neurons (n = 9–12 mice). CNO-treated control animals spend a bit more time grooming (n = 19 mice), which is suppressed by activation of Ptf1a$^+$ neurons (n = 12 mice).

Data: mean ± SEM. Two-sided Wilcoxon's signed rank paired and two-sided Mann-Whitney's unpaired U test. See also Figure S5.

triggering itch. Concomitant removal of GRPR-Cre neurons delays the maximum expression of the phenotype but does not reduce the scratching bout frequency, suggesting partial functional redundancy with another excitatory pathway.

Ptf1a-Cre Neurons Inhibit GRPR-Mediated Itch

To assess the function of Ptf1a-Cre neurons in controlling GRPR-mediated itch, we used a chemogenetic intersectional approach in which GRPR-Cre and/or Ptf1a-Cre neurons were stimulated (Sciolino et al., 2016) (Figure 6A; Figures S5A and S5B). Clozapine-N-oxide (CNO)-mediated activation of GRPR-Cre neurons induced a 20-fold increase in the number of scratching bouts compared with vehicle- or CNO-treated control animals (Figure 6B), as also recently reported using a different approach (Bardoni et al., 2018). Chemogenetic activation of inhibitory Ptf1a-Cre neurons did not elicit changes in somatosensory or motor behavior or in a conditioned place aversion assay (Figures S5C–S5K). Simultaneous activation of Ptf1a-Cre and GRPR-Cre neurons resulted in a 70% reduction in the number of scratching bouts compared with animals with only activated GRPR-Cre neurons (Figure 6B). These results suggest that Ptf1a-Cre neurons normally inhibit mechanosensory information that otherwise activates the GRPR-mediated itch circuit.

Grooming has been connected to a neuronal itch circuit (Gao et al., 2019). We observed that activation of GRPR-Cre neurons increased grooming behavior. GRPR-Cre neuron-activated animals spent 80% of the assay time grooming, compared with vehicle-treated mice (23%) (Figure 6C). Simultaneous activation of GRPR-Cre and Ptf1a-Cre neurons did not result in a significant reduction of grooming activity, suggesting that Ptf1a-Cre neurons do not control the GRPR-Cre-mediated grooming circuit. In summary, our results suggest a well-defined function for Ptf1a-Cre neurons in gating-specific mechanosensory inputs to the GRPR-mediated itch circuit, but not the grooming circuit, which is in agreement with the partial targeting of the Ptf1a-Cre mouse line described earlier.

DISCUSSION

In this study, we report that a subset of spinal presynaptic inhibitory neurons marked by expression of Ptf1a gate self-generated mechanosensory information during movement to prevent innocuous stimuli from triggering a scratch response (Figure 7). Loss of these neurons gives rise to hairy skin hypersensitivity and chronic itch. We propose that Ptf1a-controlled inhibition of cutaneous afferents in the spinal dorsal horn normally silences self-produced stimuli generated at the skin to facilitate adequate responses to externally induced stimuli.

Common Developmental Origin of Spinal Inhibitory Neurons Gating Itch Circuits

Adult loss of spinal inhibitory neurons expressing GAD65, GLYT2, or NPY leads to spontaneous scratching (Bourane et al., 2015a; Fink et al., 2014; Foster et al., 2015). Each of these genes requires Ptf1a for proper expression in the dorsal horn during neurogenesis (Borromeo et al., 2014; Huang et al., 2008; Wildner et al., 2013). Such dependency establishes a common developmental link for these subtypes to the dI4/dILA class

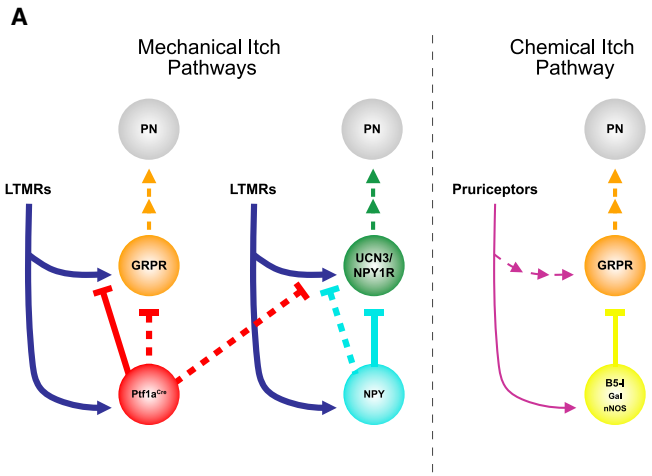

Figure 7. Itch Models

Scheme representing a simplified view of itch circuits in the spinal dorsal horn according to the literature and the present results. Inhibitory neurons that are lost in bHLH5b knockout mice (B5-I$^+$) gate the chemical itch pathway exerting inhibition upon GRPR$^+$ neurons, the central hub of chemical itch in the dorsal spinal cord. Mechanosensory information from low-threshold mechanoreceptors (LTMRs) gates NPY$^+$ neurons driving inhibition onto Ucn3$^+$ and NPY1R$^+$ neurons. NPY$^+$ presynaptic contacts were previously described upon cutaneous mechanosensory afferents in the dorsal horn (Betley et al., 2009). Ptf1a-Cre neurons gate GRPR$^+$ neuron activation through mechanosensory inputs. The identity of LTMRs and whether they are shared between mechanical pathways remains to be investigated (for a detailed molecular description of chemical versus mechanical itch pathways, see Jakobsson et al., 2019). A possible post-synaptic role for Ptf1a-Cre-derived neurons cannot be ruled out. Projection neurons (PNs) transmit itch signals to the brain. Serial arrows depict polysynaptic pathways. Dashed lines represent hypothetical connections based on the literature.

of inhibitory neurons (Cheng et al., 2004; Glasgow et al., 2005; Gross et al., 2002; Müller et al., 2002; Wildner et al., 2006). We reasoned that a common specification cascade during development might be relevant for their function in mature circuits. Indeed, all three genes have been identified as markers for presynaptic inhibitory neurons: GLYT2 and NPY neurons target cutaneous afferents, and GAD65 is believed to be important for these neurons to sustain a high inhibitory tone (Betley et al., 2009; Fink et al., 2014; Hughes et al., 2005). Sharing such characteristics, we hypothesized that using Ptf1a as a genetic entry point to manipulate the function of these inhibitory neurons together would reveal the mechanisms of presynaptic inhibition control over the itch response. Perinatal death of Ptf1a knockout mice (Glasgow et al., 2005; Hori et al., 2008) precluded any study on neuronal subtype composition of the mature dorsal horns or behavioral analysis. Here we used a Ptf1a-Cre knockin mouse line (Nakhai et al., 2007) with better recombination efficiency than the line commonly used in spinal cord studies (Kawaguchi et al., 2002). Even though we found that Ptf1a is more widely transcribed than previously reported, probably due to post-transcriptional regulation, Lmx1b$^+$ neuron numbers were not affected upon ablation. This observation has been made before using the same genetic ablation strategy (Duan et al., 2014), which suggests a bias toward inhibitory neurons that warrants further research. We found that several well-known markers of spinal inhibitory neurons, including enkephalin, galanin, nNOS, or NPY, were not affected after Ptf1a-Cre ablation. This is in agreement with recent single-cell transcriptomic studies that identified six subtypes of dI4/dILA neurons in the developing spinal cord, only one of them characterized by expression of Ptf1a (Delile et al., 2019). Consistently, NPY appeared in a different subtype. Loss of inhibitory neurons in the spinal cord leading to spontaneous scratching has been previously associated with the loss of galanin and nNOS neurons in the superficial dorsal horn of bHLH5b knockout mice (Kardon et al., 2014; Ross et al., 2010). These two subtypes of inhibitory neurons have been shown to directly inhibit GRPR neurons (Liu et al., 2019), supporting their proposed role in gating the GRPR neuron-dependent itch-signaling pathway. In agreement with our results, which show no changes in these two populations, expression of both galanin and nNOS is not affected in Ptf1a knockout mice (Borromeo et al., 2014).

Loss of Ptf1a-Cre neurons results in the most intense spontaneous-scratching phenotype reported to date (Ptf1a-Cre ablation, 22 bouts/min; GAD65-Cre ablation, 5 bouts/min; and NPY-Cre ablation, 4.2 bouts/min), and is the fastest to develop after ablation (Ptf1a-Cre, 3.7 days; GAD65-Cre, 7 days [estimated]; and NPY-Cre, 1–2 weeks) (Acton et al., 2019; Bourane et al., 2015a; Fink et al., 2014). Moreover, we confirmed the same behavioral phenotype using a second Ptf1a-Cre knockin mouse line. Our results unravel the existence of one as-yet-uncharacterized subset of inhibitory neurons in the dorsal horn with a predominant role in mechanical itch gating. Further studies to ascertain the identity of this neuron subtype would be important to map the role of each spinal inhibitory population in the regulation of itch.

Gating Self-Generated Mechanosensory Information

Our results show that Ptf1a-Cre neurons make up more than 80% of all adult presynaptic inhibitory contacts onto cutaneous mechanosensory fibers, in agreement with developmental studies (Betley et al., 2009) and their role in sensorimotor control gain (Fink et al., 2014). Presynaptic inhibition is a fundamental mechanism for the correct development of tactile sensitivity and social interactions among others (Orefice et al., 2016; Zimmerman et al., 2019). Strikingly, the link between study areas, the neurons responsible for such presynaptic inhibition at somatosensory afferents, has so far been overlooked. Here, we show that partial loss of Ptf1a neurons increases hairy skin sensitivity and leads to the development of a dramatic spontaneous-scratching phenotype, including severe skin lesions. Our analysis of this phenotype suggests that loss of presynaptic inhibition of mechanosensory afferents underlies the increased hairy skin sensitivity that gives rise to scratching. The positive correlations of animal activity with scratching frequency plus those of hair stimulation with increased dorsal horn neural activity suggest that self-generated activation of hair mechanosensory inputs during movement triggers an exacerbated scratch response in the absence of Ptf1a-Cre neuron inhibition. The presence of mechanosensory cues in the environment, such as bedding material in the home cages, increases the likelihood of hair activation: in humans, clothes contacting skin hairs represent an equivalent scenario. Lack of an acute mechanical itch

phenotype, such as that previously described for NPY-Cre neuron-ablated animals (Acton et al., 2019; Bourane et al., 2015a; Pan et al., 2019), agrees with our Ptf1a-Cre targeting data. Moreover, acute mechanical itch has been proposed to be mediated by Merkel touch-dome cells in the skin (Feng et al., 2018; Pan et al., 2019), which transmit a different type of mechanosensory information compared with hair mechanoreceptors. These results point to diverse subsets of presynaptic inhibitory neurons specialized in the gating of different mechanosensory information submodalities (Figure 7). Further studies are warranted to characterize the subtype of mechanoreceptive fibers targeted by Ptf1a-Cre neurons and to measure the possible contribution of post-synaptic inhibition in this context.

Itch and the Perception of Touch

Concomitant ablation of GRPR-Cre and Ptf1a-Cre neurons delayed the development of the scratching phenotype for more than one day. These data suggest that upon increased mechanosensory drive in the dorsal horn, GRPR neurons become activated, eliciting an itch response. It follows that GRPR neurons normally receive direct or indirect mechanosensory cutaneous information. We provide anatomical evidence for this (Figure 5B); however, it remains to be physiologically demonstrated. It has also been shown that GRPR neurons require a strong excitatory drive from GRP neurons to elicit action potential firing (Pagani et al., 2019). Considering that 90% of the body surface of mammals is covered by hairy skin (Djouhri, 2016), it is tempting to speculate that mechanosensory input to the circuit is used to maintain GRPR neurons at a high subthreshold level of excitation. Some evidence for this mechanism comes from the observation that GRPR neuronal activation (Figure 6B) (Bardoni et al., 2018) evokes not only scratching behavior but also intense grooming activity (Figure 6C), which could be the outcome of lower-level activation of GRPR neurons. The delayed-scratching phenotype reaches peak intensity, which suggests that other itch-signaling neurons, distinct from GRPR ones, become stimulated upon Ptf1a-Cre ablation. Candidates include Ucn3$^+$ and NPYR1$^+$ neurons, which were shown to be involved in mechanical itch and spontaneous scratching through an NPY gating mechanism. Both populations receive mechanosensory input, and at least for Ucn3$^+$ neurons, this input is masked through inhibition under normal conditions (Acton et al., 2019; Pan et al., 2019) (Figure 7).

Thus, Ptf1a-Cre neurons seem to be part of a wider system in charge of blocking self-generated somatosensory stimuli during ongoing motor activity. A similar system has been shown to receive higher motor commands to reduce somatosensory gain during planning and execution of limb movements (Juravle et al., 2017; Voudouris and Fiehler, 2017). In the cutaneous somatosensory system, a reduction in sensory gain is essential to ignore self-generated stimuli and allow the system to detect external, life-threatening/saving signals (Watson, 1992), and loss of such inhibition leads to chronic itch.

STAR★METHODS

Detailed methods are provided in the online version of this paper and include the following:

SUPPLEMENTAL INFORMATION

Supplemental Information can be found online at https://doi.org/10.1016/j.celrep.2020.108422.

ACKNOWLEDGMENTS

We thank the MPI animal facility for support in mouse line maintenance; Martyn Goulding (Salk Institute), Patricia Jensen (NIEHS), Silvia Arber (Biozentrum-University of Basel, Friedrich Miescher Institute), Jens Siveke (Technische Universität München), Benjamin Arenkiel (Baylor College of Medicine), and Malin Lagerström (Uppsala Universitet) for mouse lines; Thomas Müller and Carmen Birchmeier (MDC Berlin) for antibodies; Kenneth Klau and Lisa Koletsou for assistance with animal facility work; Daniel del Toro, Hakan Kucukdereli, and Amelia Douglass for constructive discussions; and Sonia Paixão and Louise Gaitanos for critical reading of the manuscript. This study was supported by funds from the Max Planck Society to R.K. and LaCaixa Banking Foundation through the Postdoctoral Junior Leader Fellowship Programme (LCF/BQ/PI18/11630005) to A.E.

AUTHOR CONTRIBUTIONS

Conceptualization, A.E. and R.K.; Methodology, A.E.; Validation, A.E. and R.K.; Formal Analysis, A.E.; Investigation, A.E.; Resources, A.E.; Data

Curation, A.E.; Writing – Original Draft, A.E. and R.K.; Writing – Review & Editing, A.E. and R.K.; Visualization, A.E.; Supervision, R.K.; Funding Acquisition, A.E. and R.K.

DECLARATION OF INTERESTS

The authors declare no competing interests.

Received: February 21, 2020
Revised: April 27, 2020
Accepted: November 2, 2020
Published: November 24, 2020

REFERENCES

Abraira, V.E., Kuehn, E.D., Chirila, A.M., Springel, M.W., Toliver, A.A., Zimmerman, A.L., Orefice, L.L., Boyle, K.A., Bai, L., Song, B.J., et al. (2017). The Cellular and Synaptic Architecture of the Mechanosensory Dorsal Horn. Cell *168*, 295–310.e19.

Acton, D., Ren, X., Di Costanzo, S., Dalet, A., Bourane, S., Bertocchi, I., Eva, C., and Goulding, M. (2019). Spinal Neuropeptide Y1 Receptor-Expressing Neurons Form an Essential Excitatory Pathway for Mechanical Itch. Cell Rep. *28*, 625–639.e6.

Alaynick, W.A., Jessell, T.M., and Pfaff, S.L. (2011). SnapShot: spinal cord development. Cell *146*, 178–178.e1.

Aresh, B., Freitag, F.B., Perry, S., Blümel, E., Lau, J., Franck, M.C.M., and Lagerström, M.C. (2017). Spinal cord interneurons expressing the gastrin-releasing peptide receptor convey itch through VGLUT2-mediated signaling. Pain *158*, 945–961.

Azim, E., Fink, A.J.P., and Jessell, T.M. (2014). Internal and External Feedback Circuits for Skilled Forelimb Movement. Cold Spring Harb. Symp. Quant. Biol. *79*, 81–92.

Babayan, B.M., and Konen, C.S. (2019). Behavior Matters. Neuron *104*, 1.

Bardoni, R., Barry, D.M., Li, H., Shen, K.-F., Jeffry, J., Yang, Q., Comitato, A., Li, Y.-Q., and Chen, Z.-F. (2018). Counter-stimuli Inhibit GRPR Neurons via GABAergic Signaling in the Spinal Cord. bioRxiv. https://doi.org/10.1101/489831.

Betley, J.N., Wright, C.V.E., Kawaguchi, Y., Erdélyi, F., Szabó, G., Jessell, T.M., and Kaltschmidt, J.A. (2009). Stringent specificity in the construction of a GABAergic presynaptic inhibitory circuit. Cell *139*, 161–174.

Borromeo, M.D., Meredith, D.M., Castro, D.S., Chang, J.C., Tung, K.C., Guillemot, F., and Johnson, J.E. (2014). A transcription factor network specifying inhibitory versus excitatory neurons in the dorsal spinal cord. Development *141*, 2803–2812.

Bourane, S., Duan, B., Koch, S.C., Dalet, A., Britz, O., Garcia-Campmany, L., Kim, E., Cheng, L., Ghosh, A., Ma, Q., and Goulding, M. (2015a). Gate control of mechanical itch by a subpopulation of spinal cord interneurons. Science *350*, 550–554.

Bourane, S., Grossmann, K.S., Britz, O., Dalet, A., Del Barrio, M.G., Stam, F.J., Garcia-Campmany, L., Koch, S., and Goulding, M. (2015b). Identification of a spinal circuit for light touch and fine motor control. Cell *160*, 503–515.

Bouvier, J., Caggiano, V., Leiras, R., Caldeira, V., Bellardita, C., Balueva, K., Fuchs, A., and Kiehn, O. (2015). Descending Command Neurons in the Brainstem that Halt Locomotion. Cell *163*, 1191–1203.

Brenner, D.S., Golden, J.P., and Gereau, R.W., 4th. (2012). A novel behavioral assay for measuring cold sensation in mice. PLoS ONE *7*, e39765.

Britz, O., Zhang, J., Grossmann, K.S., Dyck, J., Kim, J.C., Dymecki, S., Gosgnach, S., and Goulding, M. (2015). A genetically defined asymmetry underlies the inhibitory control of flexor-extensor locomotor movements. eLife *4*, e04718.

Bröhl, D., Strehle, M., Wende, H., Hori, K., Bormuth, I., Nave, K.-A., Müller, T., and Birchmeier, C. (2008). A transcriptional network coordinately determines transmitter and peptidergic fate in the dorsal spinal cord. Dev. Biol. *322*, 381–393.

Brownstone, R.M., and Chopek, J.W. (2018). Reticulospinal Systems for Tuning Motor Commands. Front. Neural Circuits *12*, 30.

Capelli, P., Pivetta, C., Soledad Esposito, M., and Arber, S. (2017). Locomotor speed control circuits in the caudal brainstem. Nature *551*, 373–377.

Chen, J.-A., Huang, Y.-P., Mazzoni, E.O., Tan, G.C., Zavadil, J., and Wichterle, H. (2011). Mir-17-3p controls spinal neural progenitor patterning by regulating Olig2/Irx3 cross-repressive loop. Neuron *69*, 721–735.

Cheng, L., Arata, A., Mizuguchi, R., Qian, Y., Karunaratne, A., Gray, P.A., Arata, S., Shirasawa, S., Bouchard, M., Luo, P., et al. (2004). Tlx3 and Tlx1 are post-mitotic selector genes determining glutamatergic over GABAergic cell fates. Nat. Neurosci. *7*, 510–517.

Cheng, L., Samad, O.A., Xu, Y., Mizuguchi, R., Luo, P., Shirasawa, S., Goulding, M., and Ma, Q. (2005). Lbx1 and Tlx3 are opposing switches in determining GABAergic versus glutamatergic transmitter phenotypes. Nat. Neurosci. *8*, 1510–1515.

Dai, J.-X., Hu, Z.-L., Shi, M., Guo, C., and Ding, Y.-Q. (2008). Postnatal ontogeny of the transcription factor Lmx1b in the mouse central nervous system. J. Comp. Neurol. *509*, 341–355.

de Chevigny, A., Coré, N., Follert, P., Gaudin, M., Barbry, P., Béclin, C., and Cremer, H. (2012). miR-7a regulation of Pax6 controls spatial origin of forebrain dopaminergic neurons. Nat. Neurosci. *15*, 1120–1126.

Delile, J., Rayon, T., Melchionda, M., Edwards, A., Briscoe, J., and Sagner, A. (2019). Single cell transcriptomics reveals spatial and temporal dynamics of gene expression in the developing mouse spinal cord. Development *146*, dev173807.

Dessaud, E., Yang, L.L., Hill, K., Cox, B., Ulloa, F., Ribeiro, A., Mynett, A., Novitch, B.G., and Briscoe, J. (2007). Interpretation of the sonic hedgehog morphogen gradient by a temporal adaptation mechanism. Nature *450*, 717–720.

Detloff, M.R., Fisher, L.C., Deibert, R.J., and Basso, D.M. (2012). Acute and chronic tactile sensory testing after spinal cord injury in rats. J. Vis. Exp. *62*, e3247.

Djouhri, L. (2016). Aδ-fiber low threshold mechanoreceptors innervating mammalian hairy skin: A review of their receptive, electrophysiological and cytochemical properties in relation to Aδ-fiber high threshold mechanoreceptors. Neurosci. Biobehav. Rev. *61*, 225–238.

Dong, X., and Dong, X. (2018). Peripheral and Central Mechanisms of Itch. Neuron *98*, 482–494.

Duan, B., Cheng, L., Bourane, S., Britz, O., Padilla, C., Garcia-Campmany, L., Krashes, M., Knowlton, W., Velasquez, T., Ren, X., et al. (2014). Identification of spinal circuits transmitting and gating mechanical pain. Cell *159*, 1417–1432.

Feng, J., Luo, J., Yang, P., Du, J., Kim, B.S., and Hu, H. (2018). Piezo2 channel-Merkel cell signaling modulates the conversion of touch to itch. Science *360*, 530–533.

Fink, A.J.P., Croce, K.R., Huang, Z.J., Abbott, L.F., Jessell, T.M., and Azim, E. (2014). Presynaptic inhibition of spinal sensory feedback ensures smooth movement. Nature *509*, 43–48.

Foster, E., Wildner, H., Tudeau, L., Haueter, S., Ralvenius, W.T., Jegen, M., Johannssen, H., Hösli, L., Haenraets, K., Ghanem, A., et al. (2015). Targeted ablation, silencing, and activation establish glycinergic dorsal horn neurons as key components of a spinal gate for pain and itch. Neuron *85*, 1289–1304.

Frost, W.N., Tian, L.-M., Hoppe, T.A., Mongeluzi, D.L., and Wang, J. (2003). A cellular mechanism for prepulse inhibition. Neuron *40*, 991–1001.

Fukuoka, M., Miyachi, Y., and Ikoma, A. (2013). Mechanically evoked itch in humans. Pain *154*, 897–904.

Gao, Z.-R., Chen, W.-Z., Liu, M.-Z., Chen, X.-J., Wan, L., Zhang, X.-Y., Yuan, L., Lin, J.-K., Wang, M., Zhou, L., et al. (2019). Tac1-Expressing Neurons in the Periaqueductal Gray Facilitate the Itch-Scratching Cycle via Descending Regulation. Neuron *101*, 45–59.e9.

Geuther, B.Q., Deats, S.P., Fox, K.J., Murray, S.A., Braun, R.E., White, J.K., Chesler, E.J., Lutz, C.M., and Kumar, V. (2019). Robust mouse tracking in complex environments using neural networks. Commun. Biol. *2*, 124.

Glasgow, S.M., Henke, R.M., Macdonald, R.J., Wright, C.V., and Johnson, J.E. (2005). Ptf1a determines GABAergic over glutamatergic neuronal cell fate in the spinal cord dorsal horn. Development *132*, 5461–5469.

Gross, M.K., Dottori, M., and Goulding, M. (2002). Lbx1 specifies somatosensory association interneurons in the dorsal spinal cord. Neuron *34*, 535–549.

Hafenreffer, S. (1660). Nosodochion : in quo cutis, eique adhaerentium partium, affectus omnes, singulari methodo et cognoscendi et curandi fidelissime traduntur. (Kühn).

Helms, A.W., and Johnson, J.E. (2003). Specification of dorsal spinal cord interneurons. Curr. Opin. Neurobiol. *13*, 42–49.

Hori, K., Cholewa-Waclaw, J., Nakada, Y., Glasgow, S.M., Masui, T., Henke, R.M., Wildner, H., Martarelli, B., Beres, T.M., Epstein, J.A., et al. (2008). A nonclassical bHLH Rbpj transcription factor complex is required for specification of GABAergic neurons independent of Notch signaling. Genes Dev. *22*, 166–178.

Huang, M., Huang, T., Xiang, Y., Xie, Z., Chen, Y., Yan, R., Xu, J., and Cheng, L. (2008). Ptf1a, Lbx1 and Pax2 coordinate glycinergic and peptidergic transmitter phenotypes in dorsal spinal inhibitory neurons. Dev. Biol. *322*, 394–405.

Hughes, D.I., Mackie, M., Nagy, G.G., Riddell, J.S., Maxwell, D.J., Szabó, G., Erdélyi, F., Veress, G., Szucs, P., Antal, M., and Todd, A.J. (2005). P boutons in lamina IX of the rodent spinal cord express high levels of glutamic acid decarboxylase-65 and originate from cells in deep medial dorsal horn. Proc. Natl. Acad. Sci. USA *102*, 9038–9043.

Ikoma, A., Handwerker, H., Miyachi, Y., and Schmelz, M. (2005). Electrically evoked itch in humans. Pain *113*, 148–154.

Jakobsson, J.E.T., Ma, H., and Lagerström, M.C. (2019). Neuropeptide Y in itch regulation. Neuropeptides *78*, 101976.

Juravle, G., Binsted, G., and Spence, C. (2017). Tactile suppression in goal-directed movement. Psychon. Bull. Rev. *24*, 1060–1076.

Kabra, M., Robie, A.A., Rivera-Alba, M., Branson, S., and Branson, K. (2013). JAABA: interactive machine learning for automatic annotation of animal behavior. Nat. Methods *10*, 64–67.

Kardon, A.P., Polgár, E., Hachisuka, J., Snyder, L.M., Cameron, D., Savage, S., Cai, X., Karnup, S., Fan, C.R., Hemenway, G.M., et al. (2014). Dynorphin acts as a neuromodulator to inhibit itch in the dorsal horn of the spinal cord. Neuron *82*, 573–586.

Kawaguchi, Y., Cooper, B., Gannon, M., Ray, M., MacDonald, R.J., and Wright, C.V.E. (2002). The role of the transcriptional regulator Ptf1a in converting intestinal to pancreatic progenitors. Nat. Genet. *32*, 128–134.

Kini, S.P., DeLong, L.K., Veledar, E., McKenzie-Brown, A.M., Schaufele, M., and Chen, S.C. (2011). The impact of pruritus on quality of life: the skin equivalent of pain. Arch. Dermatol. *147*, 1153–1156.

Lallemend, F., and Ernfors, P. (2012). Molecular interactions underlying the specification of sensory neurons. Trends Neurosci. *35*, 373–381.

Li, Y., Qiu, Q., Watson, S.S., Schweitzer, R., and Johnson, R.L. (2010). Uncoupling skeletal and connective tissue patterning: conditional deletion in cartilage progenitors reveals cell-autonomous requirements for Lmx1b in dorsal-ventral limb patterning. Development *137*, 1181–1188.

Liang, H., Watson, C., and Paxinos, G. (2016). Terminations of reticulospinal fibers originating from the gigantocellular reticular formation in the mouse spinal cord. Brain Struct. Funct. *221*, 1623–1633.

Liu, M.-Z., Chen, X.-J., Liang, T.-Y., Li, Q., Wang, M., Zhang, X.-Y., Li, Y.-Z., Sun, Q., and Sun, Y.-G. (2019). Synaptic control of spinal GRPR^{+} neurons by local and long-range inhibitory inputs. Proc. Natl. Acad. Sci. USA *116*, 27011–27017.

Madisen, L., Zwingman, T.A., Sunkin, S.M., Oh, S.W., Zariwala, H.A., Gu, H., Ng, L.L., Palmiter, R.D., Hawrylycz, M.J., Jones, A.R., et al. (2010). A robust and high-throughput Cre reporting and characterization system for the whole mouse brain. Nat. Neurosci. *13*, 133–140.

Madisen, L., Garner, A.R., Shimaoka, D., Chuong, A.S., Klapoetke, N.C., Li, L., van der Bourg, A., Niino, Y., Egolf, L., Monetti, C., et al. (2015). Transgenic mice for intersectional targeting of neural sensors and effectors with high specificity and performance. Neuron *85*, 942–958.

Mende, M., Fletcher, E.V., Belluardo, J.L., Pierce, J.P., Bommareddy, P.K., Weinrich, J.A., Kabir, Z.D., Schierberl, K.C., Pagiazitis, J.G., Mendelsohn, A.I., et al. (2016). Sensory-Derived Glutamate Regulates Presynaptic Inhibitory Terminals in Mouse Spinal Cord. Neuron *90*, 1189–1202.

Meredith, D.M., Masui, T., Swift, G.H., MacDonald, R.J., and Johnson, J.E. (2009). Multiple transcriptional mechanisms control Ptf1a levels during neural development including autoregulation by the PTF1-J complex. J. Neurosci. *29*, 11139–11148.

Misery, L., Dutray, S., Chastaing, M., Schollhammer, M., Consoli, S.G., and Consoli, S.M. (2018). Psychogenic itch. Transl. Psychiatry *8*, 52.

Mizuguchi, R., Kriks, S., Cordes, R., Gossler, A., Ma, Q., and Goulding, M. (2006). Ascl1 and Gsh1/2 control inhibitory and excitatory cell fate in spinal sensory interneurons. Nat. Neurosci. *9*, 770–778.

Mollanazar, N.K., Sethi, M., Rodriguez, R.V., Nattkemper, L.A., Ramsey, F.V., Zhao, H., and Yosipovitch, G. (2016). Retrospective analysis of data from an itch center: Integrating validated tools in the electronic health record. J. Am. Acad. Dermatol. *75*, 842–844.

Moreno-López, Y., Olivares-Moreno, R., Cordero-Erausquin, M., and Rojas-Piloni, G. (2016). Sensorimotor Integration by Corticospinal System. Front. Neuroanat. *10*, 24.

Mueller, S., Fischer, M., Herger, S., Nüesch, C., Egloff, C., Itin, P., Cajacob, L., Brandt, O., and Mündermann, A. (2019). Good vibrations: Itch induction by whole body vibration exercise without the need of a pruritogen. Exp. Dermatol. *28*, 1390–1396.

Müller, T., Brohmann, H., Pierani, A., Heppenstall, P.A., Lewin, G.R., Jessell, T.M., and Birchmeier, C. (2002). The homeodomain factor lbx1 distinguishes two major programs of neuronal differentiation in the dorsal spinal cord. Neuron *34*, 551–562.

Nakhai, H., Sel, S., Favor, J., Mendoza-Torres, L., Paulsen, F., Duncker, G.I.W., and Schmid, R.M. (2007). Ptf1a is essential for the differentiation of GABAergic and glycinergic amacrine cells and horizontal cells in the mouse retina. Development *134*, 1151–1160.

Nelson, T.S., Fu, W., Donahue, R.R., Corder, G.F., Hökfelt, T., Wiley, R.G., and Taylor, B.K. (2019). Facilitation of neuropathic pain by the NPY Y1 receptor-expressing subpopulation of excitatory interneurons in the dorsal horn. Sci. Rep. *9*, 7248.

Oetjen, L.K., Mack, M.R., Feng, J., Whelan, T.M., Niu, H., Guo, C.J., Chen, S., Trier, A.M., Xu, A.Z., Tripathi, S.V., et al. (2017). Sensory Neurons Co-opt Classical Immune Signaling Pathways to Mediate Chronic Itch. Cell *171*, 217–228.e13.

Orefice, L.L., Zimmerman, A.L., Chirila, A.M., Sleboda, S.J., Head, J.P., and Ginty, D.D. (2016). Peripheral Mechanosensory Neuron Dysfunction Underlies Tactile and Behavioral Deficits in Mouse Models of ASDs. Cell *166*, 299–313.

Orefice, L.L., Mosko, J.R., Morency, D.T., Wells, M.F., Tasnim, A., Mozeika, S.M., Ye, M., Chirila, A.M., Emanuel, A.J., Rankin, G., et al. (2019). Targeting Peripheral Somatosensory Neurons to Improve Tactile-Related Phenotypes in ASD Models. Cell *178*, 867–886.e24.

Osakada, Fumitaka, Mori, Takuma, Cetin, Ali, Marshel, James, Virgen, Beatriz, and Callaway, Edward (2011). New Rabies Virus Variants for Monitoring and Manipulating Activity and Gene Expression in Defined Neural Circuits. Neuron *71*, 617–631.

Pagani, M., Albisetti, G.W., Sivakumar, N., Wildner, H., Santello, M., Johannssen, H.C., and Zeilhofer, H.U. (2019). How Gastrin-Releasing Peptide Opens the Spinal Gate for Itch. Neuron *103*, 102–117.e5.

Pan, H., Fatima, M., Li, A., Lee, H., Cai, W., Horwitz, L., Hor, C.C., Zaher, N., Cin, M., Slade, H., et al. (2019). Identification of a Spinal Circuit for Mechanical and Persistent Spontaneous Itch. Neuron *103*, 1135–1149.e6.

Pereira, P.J.S., Machado, G.D.B., Danesi, G.M., Canevese, F.F., Reddy, V.B., Pereira, T.C.B., Bogo, M.R., Cheng, Y.-C., Laedermann, C., Talbot, S., et al. (2015). GRPR/PI3Kγ: Partners in Central Transmission of Itch. J. Neurosci. *35*, 16272–16281.

Poulet, J.F., and Hedwig, B. (2006). The cellular basis of a corollary discharge. Science *311*, 518–522.

Punnakkal, P., von Schoultz, C., Haenraets, K., Wildner, H., and Zeilhofer, H.U. (2014). Morphological, biophysical and synaptic properties of glutamatergic neurons of the mouse spinal dorsal horn. J. Physiol. *592*, 759–776.

Ross, S.E., Mardinly, A.R., McCord, A.E., Zurawski, J., Cohen, S., Jung, C., Hu, L., Mok, S.I., Shah, A., Savner, E.M., et al. (2010). Loss of inhibitory interneurons in the dorsal spinal cord and elevated itch in Bhlhb5 mutant mice. Neuron *65*, 886–898.

Rudomin, P. (2009). In search of lost presynaptic inhibition. Exp. Brain Res. *196*, 139–151.

Rudomin, P., and Schmidt, R.F. (1999). Presynaptic inhibition in the vertebrate spinal cord revisited. Exp. Brain Res. *129*, 1–37.

Schindelin, Johannes, Arganda-Carreras, Ignacio, Frise, Erwin, Kaynig, Verena, Longair, Mark, Pietzsch, Tobias, Preibisch, Stephan, Rueden, Curtis, Saalfeld, Stephan, Schmid, Benjamin, Tinevez, Jean-Yves, White, Daniel, Hartenstein, Volker, Eliceiri, Kevin, Tomancak, Pavel, and Cardona, Albert (2012). Fiji: an open-source platform for biological-image analysis. Nature Methods *9*. https://doi.org/10.1038/nmeth.2019.

Schut, C., Dalgard, F.J., Halvorsen, J.A., Gieler, U., Lien, L., Aragones, L.T., Poot, F., Jemec, G.B.E., Misery, L., Kemény, L., et al. (2019). Occurrence, Chronicity and Intensity of Itch in a Clinical Consecutive Sample of Patients with Skin Diseases: A Multi-centre Study in 13 European Countries. Acta Derm. Venereol. *99*, 146–151.

Sciolino, N.R., Plummer, N.W., Chen, Y.-W., Alexander, G.M., Robertson, S.D., Dudek, S.M., McElligott, Z.A., and Jensen, P. (2016). Recombinase-Dependent Mouse Lines for Chemogenetic Activation of Genetically Defined Cell Types. Cell Rep. *15*, 2563–2573.

Seki, K., Perlmutter, S.I., and Fetz, E.E. (2003). Sensory input to primate spinal cord is presynaptically inhibited during voluntary movement. Nat. Neurosci. *6*, 1309–1316.

Sukhtankar, D.D., and Ko, M.-C. (2013). Physiological function of gastrin-releasing peptide and neuromedin B receptors in regulating itch scratching behavior in the spinal cord of mice. PLoS ONE *8*, e67422.

Sun, Y.-G., and Chen, Z.-F. (2007). A gastrin-releasing peptide receptor mediates the itch sensation in the spinal cord. Nature *448*, 700–703.

Sun, Y.-G., Zhao, Z.-Q., Meng, X.-L., Yin, J., Liu, X.-Y., and Chen, Z.-F. (2009). Cellular basis of itch sensation. Science *325*, 1531–1534.

Szabo, N.E., da Silva, R.V., Sotocinal, S.G., Zeilhofer, H.U., Mogil, J.S., and Kania, A. (2015). Hoxb8 intersection defines a role for Lmx1b in excitatory dorsal horn neuron development, spinofugal connectivity, and nociception. J. Neurosci. *35*, 5233–5246.

Takatoh, J., Nelson, A., Zhou, X., Bolton, M.M., Ehlers, M.D., Arenkiel, B.R., Mooney, R., and Wang, F. (2013). New modules are added to vibrissal premotor circuitry with the emergence of exploratory whisking. Neuron *77*, 346–360.

Tripathi, R., Knusel, K.D., Ezaldein, H.H., Bordeaux, J.S., and Scott, J.F. (2019). The cost of an itch: A nationally representative retrospective cohort study of pruritus-associated health care expenditure in the United States. J. Am. Acad. Dermatol. *80*, 810–813.

Tripodi, M., Stepien, A.E., and Arber, S. (2011). Motor antagonism exposed by spatial segregation and timing of neurogenesis. Nature *479*, 61–66.

Ueno, M., Nakamura, Y., Li, J., Gu, Z., Niehaus, J., Maezawa, M., Crone, S.A., Goulding, M., Baccei, M.L., and Yoshida, Y. (2018). Corticospinal Circuits from the Sensory and Motor Cortices Differentially Regulate Skilled Movements through Distinct Spinal Interneurons. Cell Rep. *23*, 1286–1300.e7.

Usoskin, D., Furlan, A., Islam, S., Abdo, H., Lönnerberg, P., Lou, D., Hjerling-Leffler, J., Haeggström, J., Kharchenko, O., Kharchenko, P.V., et al. (2015). Unbiased classification of sensory neuron types by large-scale single-cell RNA sequencing. Nat. Neurosci. *18*, 145–153.

Voudouris, D., and Fiehler, K. (2017). Enhancement and suppression of tactile signals during reaching. J. Exp. Psychol. Hum. Percept. Perform. *43*, 1238–1248.

Vrontou, S., Wong, A.M., Rau, K.K., Koerber, H.R., and Anderson, D.J. (2013). Genetic identification of C fibres that detect massage-like stroking of hairy skin *in vivo*. Nature *493*, 669–673.

Wahlgren, C.F., Hägermark, O., and Bergström, R. (1991). Patients' perception of itch induced by histamine, compound 48/80 and wool fibres in atopic dermatitis. Acta Derm. Venereol. *71*, 488–494.

Watson, A.H. (1992). Presynaptic modulation of sensory afferents in the invertebrate and vertebrate nervous system. Comp. Biochem. Physiol. Part A. Physiol. *103*, 227–239.

Weisshaar, E., Szepietowski, J.C., Dalgard, F.J., Garcovich, S., Gieler, U., Giménez-Arnau, A.M., Lambert, J., Leslie, T., Mettang, T., Misery, L., et al. (2019). European S2k Guideline on Chronic Pruritus. Acta Derm. Venereol. *99*, 469–506.

Wickersham, I.R., Finke, S., Conzelmann, K.-K., and Callaway, E.M. (2007). Retrograde neuronal tracing with a deletion-mutant rabies virus. Nat. Methods *4*, 47–49.

Wildner, H., Müller, T., Cho, S.-H., Bröhl, D., Cepko, C.L., Guillemot, F., and Birchmeier, C. (2006). dILA neurons in the dorsal spinal cord are the product of terminal and non-terminal asymmetric progenitor cell divisions, and require Mash1 for their development. Development *133*, 2105–2113.

Wildner, H., Das Gupta, R., Bröhl, D., Heppenstall, P.A., Zeilhofer, H.U., and Birchmeier, C. (2013). Genome-wide expression analysis of Ptf1a- and Ascl1-deficient mice reveals new markers for distinct dorsal horn interneuron populations contributing to nociceptive reflex plasticity. J. Neurosci. *33*, 7299–7307.

Yosipovitch, G., and Bernhard, J.D. (2013). Clinical practice. Chronic pruritus. N. Engl. J. Med. *368*, 1625–1634.

Zimmerman, A.L., Kovatsis, E.M., Pozsgai, R.Y., Tasnim, A., Zhang, Q., and Ginty, D.D. (2019). Distinct Modes of Presynaptic Inhibition of Cutaneous Afferents and Their Functions in Behavior. Neuron *102*, 420–434.e8.

STAR★METHODS

KEY RESOURCES TABLE

REAGENT or RESOURCE	SOURCE	IDENTIFIER
Antibodies		
Goat polyclonal Pax2 (1:500)	R&D Systems	Cat# AF3364; RRID:AB_10889828
Guinea pig polyclonal Lmx1B (1:10000)	C. Birchmeier (MDC, Berlin)	N/A
Rat polyclonal mCherry (1:1500)	Thermo Fisher Scientific	Cat# M11217; RRID:AB_2536611
Chicken polyclonal GFP (1:2000)	Aves-Labs	Cat# GFP-1010; RRID:AB_2307313
Chicken polyclonal B-galactosidase (1:1000)	Abcam	Cat# ab9361; RRID:AB_307210
Rabbit polyclonal Neurofilament 200 (1:1000)	Affiniti	Cat# NA1211; RRID:AB_2052006
Goat polyclonal TrkC (1:500)	R&D Systems	Cat# AF1404; RRID:AB_2155412
Rabbit monoclonal c-Fos (9F6) (1:2000)	Cell Signaling Technology	Cat# 2250S; RRID:AB_2247211
Rabbit polyclonal c-Fos (1:2000)	Santa Cruz	Cat# sc-52; RRID:AB_2106783
Sheep polyclonal TH (1:1000)	Millipore	Cat# AB1542; RRID:AB_90755
Guinea pig polyclonal vGluT2 (1:1000)	Millipore	Cat# AB2251; RRID:AB_1587626
Guinea pig polyclonal vGluT1 (1:1500)	Millipore	Cat# AB5905; RRID:AB_2301751
Rabbit polyclonal DsRed (1:1000)	Clontech	Cat# 632496; RRID:AB_10013483
Goat polyclonal CGRP (1:500)	Abcam	Cat# 36001; RRID:AB_725807
Rabbit polyclonal NPY (1:1000)	Peninsula Laboratories	Cat# T-4070.0050; RRID:AB_518504
Goat polyclonal nNOS (1:1000)	Abcam	Cat# ab1376; RRID:AB_300614
Rabbit polyclonal vGAT (1:1000)	Synaptic Systems	Cat# 131002; RRID:AB_887871
Rabbit polyclonal Enk (1:1000)	Immunostar	Cat# 20065; RRID:AB_572250
Mouse monoclonal GAD6 (1:50)	DSHB	Cat# GAD6; RRID:AB_2314499
Rabbit polyclonal Galanin (1:1000)	BMA Biomed	Cat# T-4334; RRID:AB_518348
Rabbit polyclonal RFP (1:1000)	Rockland	Cat# 600-401-379; RRID:AB_2209751
Goat polyclonal PV (1:2000)	SWANT	Cat# PVG-213; RRID:AB_2650496
Bacterial and Virus Strains		
EnvA ΔG rabies-eGFP	Viral Vector Core, Salk Institute (Osakada et al., 2011)	Addgene#32635; RRID:Addgene_32635
Chemicals, Peptides, and Recombinant Proteins		
Compound 48/80	Sigma-Aldrich	Cat# C2313
RC-3095	Sigma-Aldrich	Cat# R9653; CAS: 138147-78-1
Chloroquine diphosphate salt	Sigma-Aldrich	Cat# C6628; CAS:50-63-5
Clozapine-N-oxide	Sigma-Aldrich	Cat# C0832; CAS:34233-69-7
Diphtheria Toxin, Unnicked, from *Corynebacterium diphtheriae*	List Biological Laboratories	Cat# 150
Diphtheria Toxin from *Corynebacterium diphtheriae*	Sigma-Aldrich	Cat# D0564
Isolectin GS-IB4 From Griffonia simplicifolia, Alexa Fluor 647 Conjugate	Thermo Fisher Scientific	Cat# I32450
NeuroTrace 640/660	Thermo Fisher Scientific	Cat# N21483; RRID:AB_2572212
Experimental Models: Organisms/Strains		
Mouse: *Ai9*	The Jackson Laboratory	Cat# JAX:007909; RRID:IMSR_JAX:007909
Mouse: *Ai65D*	The Jackson Laboratory	Cat# JAX:021875; RRID:IMSR_JAX:021875
Mouse: *Ptf1a-Cre^{EX1}*	Nakhai et al., 2007	N/A
Mouse: *Ptf1a-Cre^{CVW}*	Kawaguchi et al., 2002	N/A

(*Continued on next page*)

Continued

REAGENT or RESOURCE	SOURCE	IDENTIFIER
Mouse: *Lmx1b-Cre*	Li et al., 2010	N/A
Mouse: *GRPR-Cre*	Aresh et al., 2017	N/A
Mouse: *RΦGT*	Takatoh et al., 2013	Cat# JAX:024708; RRID:IMSR_JAX:024708
Mouse: *Tau*$^{lox\text{-}stop\text{-}lox\text{-}SynGFP}$	Tripodi et al., 2011	N/A
Mouse: *Rosa26*$^{CAG\text{-}ds\text{-}hM3Dq}$	Sciolino et al., 2016	Cat# JAX:026942; RRID:IMSR_JAX:026942
Mouse: *Tau*$^{ds\text{-}DTR}$	Duan et al., 2014	N/A
Mouse: *Cdx2-FlpO*	Britz et al., 2015	N/A
Software and Algorithms		
Python	Python Software Foundation	https://www.python.org/
Ethovision XT 11	Noldus	N/A
Adobe Photoshop CS6	Adobe	N/A
Fiji (ImageJ)	Schindelin et al., 2012	https://imagej.net/Fiji
ImageJ Cell Counter Plugin	Kurt de Vos, Univ. of Sheffield, UK	https://imagej.nih.gov/ij/plugins/cell-counter.html
MATLAB	The MathWorks	N/A

RESOURCE AVAILABILITY

Lead contact

Further information and requests for resources and reagents should be directed to and will be fulfilled by the Lead Contact, Rüdiger Klein (rklein@neuro.mpg.de)

Materials availability

This study did not generate new unique reagents.

Data and Code availability

The data that support the findings of this study are available from the corresponding authors upon reasonable request. All custom-written Python and MATLAB codes used in this study are available from the corresponding authors.

EXPERIMENTAL MODEL AND SUBJECT DETAILS

Mouse lines

The mouse lines used in this study were previously described: Ptf1a-Cre^{EX1} (also known as p48^{Cre}) (Nakhai et al., 2007); Ptf1a-Cre^{CVW} (Kawaguchi et al., 2002); Tau$^{lsl\text{-}SynaptophysinGFP}$ (Tripodi et al., 2011); Ai9$^{lsl\text{-}tdTomato}$ (B6.Cg-Gt(ROSA)26Sor$^{tm9(CAG\text{-}tdTomato)Hze}$/J) (Madisen et al., 2010); Cdx2-FlpO (Britz et al., 2015); Lmx1b-Cre (Li et al., 2010); Tau$^{ds\text{-}DTR}$ (Duan et al., 2014); Rosa26$^{CAG\text{-}ds\text{-}hM3Dq}$ (Sciolino et al., 2016); Ai65D$^{ds\text{-}tdTomato}$ (B6;129S-Gt(ROSA)26Sor$^{tm65.1(CAG\text{-}tdTomato)Hze}$/J) (Madisen et al., 2015); RΦGT (Takatoh et al., 2013); GRPR-iCre (Aresh et al., 2017). All lines were backcrossed to C57BL/6J mice at least 5 generations.

Animal statement

All procedures were approved by the government of Upper Bavaria (License number 55.2-1-54-2532-130-2015) and animals were kept and used in accordance with regulations from the government of Upper Bavaria. Mice were housed on a 12 hr light/dark cycle with *ad libitum* access to food and water. All control animals were littermates, and thus all had the same genetic background and subjected to the same treatments. Adult mice (P56-90) were used for all experiments. Both male and female mice were used.

METHOD DETAILS

Monosynaptic rabies virus tracings

Adult mice were anesthetized with isofluorane (2%) and placed in a stereotaxic frame (SR-5M-HT, Narishige) with a heating pad. Anesthesia was maintained throughout the procedures at 1.5% with a nose mask (GM-4, Narishige). The analgesics Metamizol (0.2 mg/g bodyweight, oral) and Carprofen (5mg/kg bodyweight, subcutaneous) were administrated. After incision of the skin and removal of dorsal intervertebral muscles, the vertebral column was fixed with a spinal column clamp (STS-A, Narishige). A laminectomy was performed at the C2 or L1 levels, the dura matter was carefully perforated with a fine needle to expose the spinal cord. 300

nL of virus were injected unilaterally on the dorsal spinal cord 500 μm lateral to the medial artery with a fine glass capillary using a microcontroller. The skin was then closed using a Reflex 7 skin closure system and tissue adhesive (3M Vetbond). Animals were perfused 6 days post-infection. The EnvA G-deleted rabies-GFP (Wickersham et al., 2007) were produced by the Viral Vector Core of the Salk Institute.

Histology

Animals were deeply anesthetized with ketamine/xylazin (100 mg/kg and 16 mg/kg respectively) and transcardially perfused first with phosphate-buffered saline (PBS) and then with 4% paraformaldehyde (PFA) in PBS. Brains and spinal cords were dissected, post-fixed at 4°C in 4% PFA overnight, washed in PBS and embedded in 4% agarose. 70- to 100-μm sections were cut with a vibratome (Leica) and sections stored in cryoprotective solution (40% PBS, 30% glycerol, 30% ethylene glycol) at −20°C until use. Embryonic spinal cords were dissected and fixed in 4% PFA in PBS for 2h and processed as described above. DRGs were cryopreserved sequentially in 15% and 30% sucrose in PBS at 4°C, embedded in O.C.T (Fisher Scientific) and cut in a cryostat (Leica). 30 μm sections were mounted on slides, air-dried and stored at −80°C.

Immunohistochemistry

For immunofluorescence, vibratome free-floating sections and cryosections were blocked and permeabilized with 5% donkey serum, 0.3% Triton X-100 in PBS for 2 hours at room temperature (RT), following incubation with primary antibodies overnight at 4°C in 0.3% Triton X-100 in PBS. The following primary antibodies were used: goat anti-Pax2 (1:500) (AF3364, R&D Systems, RRID:AB_10889828), guinea pig anti-Lmx1b (1:10,000) (gift from C. Birchmeier, Max Delbrück Center for Molecular Medicine, Germany), rabbit anti-cFos (1:2000) (sc-52, Santa Cruz), rabbit monoclonal anti-cFos (1:2000) (2250S, Cell signaling), rat anti-mCherry (1:1500) (M11217, Thermo Fisher Scientific), chicken anti-GFP (1:2000) (GFP-1010, Aves-Labs), chicken anti-βgalactosidase (1:1000) (ab9361, Abcam,), rabbit anti-NF (1:1000) (NA1211, Affiniti), goat anti-TrkC (1:500) (AF1404, R&D Systems), sheep anti-TH (1:1000) (AB1542, Millipore), guinea pig anti-vGluT2 (1:1000) (AB2251, Millipore), guinea pig anti-vGluT1 (1:1500) (AB5905, Millipore), rabbit anti-DsRed (1:1000) (632496, Clontech), goat anti-CGRP (1:500) (36001, Abcam), rabbit anti-NPY (1:1000) (T-4070.0050, Peninsula Laboratories), goat anti-nNOS (1:1000) (ab1376, Abcam), rabbit anti-vGAT (1:1000) (131002, Synaptic Systems), rabbit anti-ENK (1:1000) (20065, Immunostar), mouse anti-GAD65 (1:50) (GAD6, Developmental Studies Hybridoma Bank, created by the NICHD of the NIH and maintained at The University of Iowa, Department of Biology, Iowa City, IA 52242), rabbit anti-Galanin (1:1000) (T-4334, BMA Biomed), rabbit anti-RFP (1:1000) (600-401-379, Rockland). After three 10-min washes in PBS, sections were incubated with secondary antibodies for 2 h at room temperature in 0.3% Triton X-100 PBS. The following secondary antibodies or counterstains were used: donkey anti-rabbit/mouse/goat/sheep/rat/chicken/guinea pig conjugated to Alexa Fluor 488, Cy3, Alexa Fluor 647 or Cy5 (1:500), Neurotrace 640/660 (1:200) (N-21483, Molecular Probes) or DAPI (1:1000). After three 15-min washes in PBS, sections were mounted in slides and coverslipped with mowiol mounting medium.

Microscopy

Fluorescence z stack images were acquired with an Olympus FV1000 or Leica SP8 confocal microscope. Images were minimally processed with FiJi/ImageJ software (NIH) or Adobe Photoshop to enhance brightness and contrast. No filters were used to decrease noise. Co-localization analysis quantification was done in single confocal z sections. Measurements were performed using FiJi/ImageJ software.

For analysis of GFP co-localization with vGAT in presynaptic puncta we followed previously described methods (Abraira et al., 2017). In short, 20-60 dorsal horn randomly selected vGlut1/vGAT appositions were marked in ImageJ per hemisection without visualizing the GFP channel. Percentages of vGlut1/vGAT appositions in which the vGAT terminal was also GFP were calculated after revealing the GFP channel. For analysis of vGlut1/vGAT appositions in DT treated animals, 50 randomly selected vGlut1 terminals were marked in ImageJ per hemisection without visualizing the vGAT channel. Percentages of vGlut1 terminals apposedby vGAT synapses were calculated after revealing the vGAT channel.

Spatial distribution of neurons

The position of interneurons in the spinal cord was recorded manually in FiJi/ImageJ. Cartesian coordinates for each interneuron were determined in the transverse spinal cord plane with respect to the midpoint of the central canal, defined as position (0,0). Custom Python scripts were used to calculate the probability density function and display two-dimensional kernel density estimations for each cell population. Estimates were graphically displayed as line contour plots, with lines connecting points of equal probability density.

Pharmacological treatments

Cell ablation was induced by intraperitoneal administration of diphtheria toxin at 50ng/g of body weight (D0564, Sigma-Aldrich) in saline solution. Injection was performed twice with a 72 hour interval (Acton et al., 2019; Bourane et al., 2015a; Duan et al., 2014; Pan et al., 2019) to both control and experimental groups. GRPR antagonist RC-3095 (Sigma-Aldrich) was dissolved in 0.1% DMSO in saline to 2μg/μl and injected intraperitoneally at 10μg/g of body weight 30 minutes before behavioral evaluation. DREADD

activation was induced by intraperitoneal injection of CNO (C0832, Sigma-Aldrich) at 2ng/g of body weight diluted in vehicle (2% DMSO in saline) to both control and experimental groups, behavioral tests were performed 30 minutes later.

Behavioral assays

Animals were acclimated to the behavioral room and testing apparatus during three consecutive days for at least 30 minutes unless otherwise indicated. Efforts were made to remain blind to the genotype of the tested animals, however given the obvious nature of the phenotype in Ptf1a-ablated animals it was not always possible. Littermates of either sex were used in all tests. Control animals lacked one of the recombinases (Cre or FlpO), except for double Ptf1a-Cre; GRPR-Cre experiments where control animals were those lacking either Cdx2-FlpO or both Ptf1a-Cre and Grpr-Cre. Except for the hot plate and rotarod, all the testing apparatuses were custom designed and built from acrylic. Schematic drawings are available upon request.

Home cage video recording (as in Figures 3A, 3B, and 3G, …)

Animals were singly housed at least one week before DT treatment. Before DT1, animals in their home cages were video recorded from the top, with cage lid and food tray removed. A transparent lamina of acrylic was used to prevent animals from getting out. Mice were recorded in pairs for 10 minutes. To evaluate the influence of bedding material in spontaneous scratching behavior, a clean cage without bedding was stacked inside the home cage to preserve as much as possible olfactory and visual cues. The double cage was returned to the rack for 30 minutes and another video recording of 10 minutes was acquired. To evaluate the role of GRPR neurons in Ptf1a neuron-mediated scratching, mice were injected with the GRPR antagonist RC-3095, returned to the double cage and rack for 30 minutes and another video recording of 10 minutes was acquired. Both scratching frequency and grooming time were calculated offline. To evaluate the influence of animal activity on scratching behavior (Figures 4J and 4K), Ptf1a-Cre neuron-ablated mice at peak scratching frequency and control littermates were recorded in their home cages as described above, which represents an active state given that the animal continuously explores the open cage. Then food tray and lid were placed back on the cage and the cage returned to the stabulation rack. 30 minutes later, animals normally default to a resting state after recovering their normal environment. Animals were recorded again without altering the cage whatsoever.

Chemical itch

Animals were lightly anesthetized with isofluorane and injected in the back skin at the level of thoracic vertebrae 12. Compound 48/80 (100 ug, Sigma-Aldrich) or chloroquine (200 ug, Sigma-Aldrich) in 50 uL of sterile saline were injected. Animals were video recorded for 30 minutes and the scratching bouts after injection counted.

Hairy skin sensitivity

To evaluate changes in hairy skin sensitivity at different air puff intensities we adapted a previously published protocol (Orefice et al., 2016). We used a SR-LAB startle response system (SDI-2325-0400, San Diego Instruments) adapted to deliver air puffs (SDI-2325-0368) to the back of the animal. Response of the animal in the form of sudden shake ("startle response") was recorded by a piezoelectric accelerometer at the base of the animal enclosure platform. Pressure regulation was achieved through a forward pressure reducing regulator (4136ANNKE, Equilibar). Animals were habituated for 10 minutes to the holding cylinder, noise and light levels the day before testing. Continuous white noise level was set to 90dB to prevent mice from hearing the opening of the pressure valve. The protocol consisted of 5 min acclimation, followed by 7 trains of 5 air puffs each delivered at pseudorandom interstimulus intervals at increasing pressures from 0.05 PSI to 2.5 PSI.

Hair stimulation of neuronal activity

To assess the ability of hair movement to induce neuronal activity in the spinal dorsal horn, we adapted a previously published protocol (Duan et al., 2014). We kept mice under light anesthesia (1%–1.5% isofluorane) using a head mask. Manipulation of the animal was reduced to the minimum possible to avoid confounding stimulations. The back hairs of the animal were combed with a soft paintbrush (#6) rostrocaudally and caudorostrally from the forelimbs to the hindlimbs for 150 times in 5 minutes. This protocol was applied 3 times with 1 minute intertrials (450 strokes in total during 17 minutes). Care was taken to avoid stimulating the skin directly. After stimulation, animals were kept under anesthesia for 2 hours, transcardially perfused and processed as previously described for cFos immunostaining.

Dynamic brush

Light touch sensitivity was evaluated with the dynamic light brush test (Bourane et al., 2015a). Mice were placed in individual compartments of a testing apparatus with a wire mesh floor. The plantar surface of the hindpaw was lightly stimulated with a soft brush (#6) stroking from heel to toe. Stimulation was repeated 10 times on alternating sides and the percentage of paw withdrawal were calculated.

Von Frey

This test was used to assess sensitivity to static touch and mechanical pain. Mice were placed in individual compartments of a testing apparatus with a wire mesh floor. Calibrated von Frey monofilaments (0.02-2 g) (Aesthesio Precision Tactile Sensory Evaluator) were

used to stimulate the medial plantar surface of the hindpaws. Withdrawal, licking or biting following or immediately after the 5 s stimulus were considered as a positive response. Paw withdrawal threshold (PWT) were calculated according to Detloff et al. (2012).

Pinprick

This test was used to evaluate mechanical pain. Mice were placed in individual compartments of a testing apparatus with a wire mesh floor. The plantar surface of the hindpaw stimulated with an Austerlitz insect pin (0.02 mm; Fine Science Tools). Stimulation was repeated 10 times on alternating sides and the percentage of paw withdrawal were calculated.

Dynamic hot plate

Heat sensitivity was evaluated through determination of the thermal withdrawal threshold. Mice were acclimated to the testing apparatus (IITC Life Science) set at 32°C the day before and the testing day for 10 minutes. The assay consisted on 3 trials in which the plate temperature increased from 32°C to 55°C at a rate of 3°C/minute. The ramp was stopped when the animals licked, shooked the hindpaw or jumped.

Cold plantar assay

Cold sensitivity was measured as previously described (Brenner et al., 2012). Mice were placed in individual compartments of a testing apparatus with a 4 mm glass floor. A pellet of crushed dry ice was positioned in contact with the glass beneath the hindpaw. The stimulus was presented 6 times on alternating sides. Latency to withdrawal was measured.

Acute mechanical itch

We performed two versions of this test, one applying the stimulus to the shaved nape of the neck (Bourane et al., 2015a) and another one to the shaved back of the animal. Mice were placed in individual compartments of a testing apparatus with a wire mesh floor and after 30 minute habituation, received five separate stimuli for ~1 s at random sites on the skin of the target region with a von Frey monofilament of 0.07 g. Scratching of the poked site was considered a positive response.

Rotarod

An accelerating rotarod (Ugo Basile) test was used to evaluate gross motor coordination. Mice were trained on 2 consecutive days at a constant speed of 5 rpm for 5 minutes. The training was repeated until each animal stayed in the cylinder without falling down for the whole 5 minutes. The third day the rotarod was programmed to accelerate from 5 to 40 rpm in 5 minutes. Each animal was subject to 3 trials with an intertrial recovery of 15 minutes. Latency to fall, maximum speed and distance walked were registered for each animal.

Open field

Overall locomotor activity and anxiety was evaluated in a custom-made acrylic 40x40x25 cm square arena. Mice were free to explore it for 15 minutes. Mean speed, distance traveled and time spent in the center of the arena (defined as a central 20x20 cm area) was measured with Ethovision XT 11 (Noldus).

Startle reflex/Prepulse inhibition (PPI)

PPI testing was performed essentially as previously described (Orefice et al., 2016, 2019) with some modifications. The tests were carried out on the same setup used for testing hairy skin sensitivity. Here we evaluated the ability of a tactile pre-stimulus (0.9 PSI, 50 ms) to inhibit startle to a stronger tactile stimulus (3 PSI, 5 ms) (tactile-tactile PPI test) or to a loud acoustic stimulus (120 dB, 20 ms) (tactile-acoustic PPI test) with an interstimulus interval of 250 ms. We sought to investigate whether Ptf1a- or GRPR-ablated animals exhibit specific tactile sensorimotor gating deficits. Animals were habituated for 10 minutes to the holding cylinder, noise and light levels the day before testing. Both PPI test versions were carried out on different days. On testing day, mice were placed inside the ventilated, cylindrical holder on a platform within a soundproof chamber. Protocols were as described (Orefice et al., 2016): acclimation phase with constant white noise (90 dB) for 5 minutes, block I, block II, block III and block IV trials. All stimuli were pseudorandomly spaced between 15 and 45 s. Block I consisted of 5 startle stimuli alone (3 PSI 5 ms or 120 dB white noise for tactile-tactile and tactile-acoustic sessions, respectively), to measure the initial startle reflex. Block II consisted of 5 prepulse stimuli alone (0.9 PSI 50 ms), to measure response to the prepulse stimulus alone. Block III incorporated prepulse/pulse, pulse alone and no stimulation trials. Block IV consisted of 5 startle stimuli alone, to measure habituation. Whole body flinch, or startle reflex, was quantified using an accelerometer sensor measuring the amplitude of movement of the animal within the cylindrical holder.

Long-term surveillance of mice in home cages

The plans for the modified cage lid, infrared LED array, camera, lens, raspberry pi and acquisition code are available upon request. We modified the cage lid for adapting a NoIR PiCamera with a modified M12 220° lens (RP-VC1N, Entaniya) to have direct view of the whole inner space of the home cage. The camera was attached to a Raspberry Pi 3 Model B (Raspberry Pi Foundation) running Raspbian and the picamera python interface was used to control acquisition and saving of the video stream. An acrylic enclosure was custom built to fit around the home cage and fitted with 5 m of an 850 nm infrared LED strip (Solarox IR1-60-850, LED1.de). Acrylic diffusers were set in place between the LED strip and the cage walls. Mice were habituated for 24 hours to the enclosure after DT2

and recording started. Video recording was stopped when Ptf1a-animals reached peak scratching frequency. FFmpeg was used to convert raw h264 movie streams to compressed video. A neural network was trained on 2000 frames labeled manually with the position and orientation of the mouse to generate an accurate elipse-fit around the mouse (Geuther et al., 2019) and track all the videos. Output of the trained neural network was used to generate the input data necessary for JAABA (Kabra et al., 2013) and train a behavior classifier to identify frames in which mice engaged in scratching behavior with the hindpaws. The resulting behavior classifier had an accuracy of 88.4% for scratch frames and 78% for non-scratch frames in videos it had never been trained on (ground-truth). This classifier was applied to all the videos for each animal. Scratching time and speed of the animals were computed (Figures S3A and S3B).

Scratching in a locomotion-restrictive context (Figures 4L and 4M)

To evaluate the influence of animal movement on scratching frequency, Ptf1a-Cre neuron-ablated mice at peak scratching frequency and control littermates were recorded in their home cages (see above) and 30 minutes later inside the same holding cylinder used in the startle reflex system. Animals were habituated for 10 minutes the day before testing and recorded for 10 minutes on testing day. Scratching frequency was quantified offline.

Conditioned Place Aversion (CPA)

To test for the valence associated with chemogenetic activation of Ptf1a-derived neurons we performed a CPA test as previously described (Vrontou et al., 2013). We designed a custom made acrylic 2-chamber arena (each chamber 15x15x30 cm, connected through a 5x5 cm opening that could be closed). Each chamber was designed with a different pattern of alternating black and white stripes (vertical or horizontal) and different patterned floor to help mice to distinguish each chamber during conditioning. On the first day, mice were free to explore both chambers for 30 minutes (Pre-Test). Conditioning started on the second day, confining the mouse to the initially preferred (IP) chamber with CNO treatment for 30 minutes. The third day, the mouse was confined to the initially non-preferred chamber (INP) after administration of vehicle. The fourth and fifth day, the cycle was repeated. On the sixth day, the mouse was allowed to explore freely both chambers and preference was calculated (Post-Test). Percentage of time spent in each chamber was assessed using Ethovision XT 11 software (Noldus).

Chemogenetic induction of itch and grooming

To evaluate itch and grooming induced behaviors by DREADD-mediated activation, mice treated with vehicle or CNO in consecutive days were placed in individual compartments of a testing apparatus with a wire mesh floor. A bottom-up view of the animals was video recorded for offline quantification. Scratching bouts and grooming time were calculated for 30 and 10 minutes, respectively, 30 minutes after treatment.

QUANTIFICATION AND STATISTICAL ANALYSIS

No statistical methods were used to predetermine sample sizes. Data presented as bar graphs indicate mean ± SEM (standard error of the mean). Dots in bar graphs and boxplots represent individual values per mouse, horizontal line indicates median. Statistical analyses were performed in Python and MATLAB using custom scripts. Significance levels are indicated as follows: $^{ns}p > 0.05$; *$p < 0.05$; **$p < 0.01$; ***$p < 0.001$; ****$p < 0.0001$. Two-sided Student́s unpaired t test was used unless otherwise noted.